Novel Ring Resonator-Based Integrated Photonic Beamformer for Broadband Phased Array Receive Antennas—Part I: Design and Performance Analysis

Arjan Meijerink, *Member, IEEE*, Chris G. H. Roeloffzen, *Member, IEEE*, Roland Meijerink, *Student Member, IEEE*, Leimeng Zhuang, *Student Member, IEEE*, David A. I. Marpaung, *Student Member, IEEE*, Mark J. Bentum, *Senior Member, IEEE*, Maurizio Burla, *Student Member, IEEE*, Jaco Verpoorte, Pieter Jorna, Adriaan Hulzinga, and Wim van Etten, *Senior Member, IEEE*

Abstract—A novel optical beamformer concept is introduced that can be used for seamless control of the reception angle in broadband wireless receivers employing a large phased array antenna (PAA). The core of this beamformer is an optical beamforming network (OBFN), using ring resonator-based broadband delays, and coherent optical combining. The electro-optical conversion is performed by means of single-sideband suppressed carrier modulation, employing a common laser, Mach-Zehnder modulators, and a common optical sideband filter after the OBFN. The unmodulated laser signal is then re-injected in order to perform balanced coherent optical detection, for the opto-electrical conversion. This scheme minimizes the requirements on the complexity of the OBFN, and has potential for compact realization by means of full integration on chip. The impact of the optical beamformer concept on the performance of the full receiver system is analyzed, by modeling the combination of the PAA and the beamformer as an equivalent two-port RF system. The results are illustrated by a numerical example of a PAA receiver for satellite TV reception, showing that—when properly designed—the beamformer hardly affects the sensitivity of the receiver.

Index Terms—Noise analysis, optical beamforming, optical ring resonators, optical SSB modulation, phased array antennas, RF photonics.

A. Meijerink, C. G. H. Roeloffzen, L. Zhuang, D. A. I. Marpaung, M. J. Bentum, and M. Burla are with the Telecommunication Engineering Group, Faculty of Electrical Engineering, Mathematics and Computer Science, University of Twente, 7500 AE Enschede, The Netherlands (e-mail: a.meijerink@ieee.org; c.g.h.roeloffzen@utwente.nl; l.zhuang@utwente.nl; d.a.i.marpaung@utwente.nl; m.j.bentum@utwente.nl; m.burla@utwente.nl).

R. Meijerink was with the Telecommunication Engineering Group, Faculty of Electrical Engineering, Mathematics and Computer Science, University of Twente, 7500 AE Enschede, The Netherlands. He is now with the Herbert Vissers College, 2150 AC Nieuw-Vennep, The Netherlands (e-mail: r.meijerink@alumnus.utwente.nl).

J. Verpoorte, P. Jorna, and A. Hulzinga are with the National Aerospace Laboratory NLR, Anthony Fokkerweg 2, 1006 BM Amsterdam, The Netherlands (e-mail: verpoor@nlr.nl; jornap@nlr.nl; hulzinga@nlr.nl).

W. van Etten, retired, was with the Telecommunication Engineering Group, Faculty of Electrical Engineering, Mathematics and Computer Science, University of Twente, 7500 AE Enschede, The Netherlands (e-mail: etten@ieee.org).

Digital Object Identifier 10.1109/JLT.2009.2029705

I. Introduction

PHOTONIC beamforming in phased array antennas (PAAs) is an interesting example of applying optical technology in wireless transmission systems. A PAA consists of an array of multiple antenna elements (AEs), corresponding transmission and/or reception units, and a beamformer, enabling direction-sensitive transmission and/or reception of electromagnetic waves [1]. In receive mode each individual AE signal consists of a time-delayed version of some desired signal, possible time-delayed versions of undesired signals (from different directions), and noise (sky noise and antenna noise). The values of these time delays are different for each AE, and depend on the geometrical distribution of the AEs and the direction(s) of the incoming wave front(s). The beamformer therefore consists of a delay-and-combine network that equalizes the delay values of the signal terms that correspond to the desired received signal, such that the desired signal terms add up in phase and are reinforced, whereas the undesired signal terms do not add up in phase and are hence suppressed. (Although some people would use the terms *beamformer* and *beamforming network* exclusively for PAAs in transmission mode, it is widely accepted to use them for receive mode as well, so we also do that in this paper.) In many applications it is desirable that the time delays are tunable, in order to be able to alter the reception angle of the PAA. When the amplitudes of the AE signals are also controlled, the shape of the beam pattern can be altered as well, for example to minimize sidelobes. PAAs offer several advantages when compared to mechanically steered antennas, such as agile beam steering, relatively low maintenance costs, reduced drag when applied in for instance vehicles or aircraft, and the possibiliy of supporting multiple antenna beams [1].

Implementing the beamformer in the optical domain shares many common advantages with other RF photonic signal processing techniques [2]–[4], such as compactness and low weight (particularly when integrated on a chip), low loss, large instantaneous bandwidth, and inherent immunity to electromagnetic interference. Optical beamforming has regained interest recently as a result of several technological developments in the last decade. Significant advances have been made in improving the performance and reducing the costs of analog optical modulators and detectors, because of widespread

interest in RF photonic links. Also, the worldwide deployment of optical fiber backbones and the more recent development of fiber-to-the-home networks has driven the state-of-the-art in planar optical circuit technology to a mature level; rather complex optical chips with low insertion losses can now be fabricated at relatively low costs [5].

Various optical beamformer concepts have been previously reported [6]. Among others, they are based on optical phase shifters [7], switchable delay matrices (using fiber optics [8] or integrated devices [9]), liquid crystal polarization switching devices [10], [11], or a combination of a wavelength-tunable laser and a dispersive optical element, such as a high-dispersion fiber [12], a fiber optic prism [13], [14], a fiber-bragg gratings (FBGs) prism [15], [16], or chirped FBGs [17]–[19]. However, phase shifters only provide the proper delay compensation at one particular frequency, and therefore result in a frequency-dependent beam angle (beam squint). This will be a problem when the PAA consists of a large number of AEs and operates over a large instantaneous bandwidth. Switchable delay matrices provide true time delays and are therefore inherently broadband, but they only allow tuning in discrete steps. In fact they show a trade-off between beam angle resolution and complexity. (This, however, could be solved using a hybrid analog-digital variable fiber-optic delay line [20], [21].) The beamformers based on the liquid crystal switching devices provide true time delays but the realized systems are bulky. The beamformers with dispersive elements offer both seamless tunability and broadband delay compensation but the delay tuning in these schemes requires bulky optical components (fibers and FBGs) and (relatively expensive) tunable lasers. The costs of these tunable lasers might not be an issue when each tunable laser illuminates multiple optical delay elements (as is done in the proposed schemes), but this results in an inherent linear relation between the tuned delays, hence limiting the applicability of the proposed schemes to linear arrays.

In this paper a seamlessly tunable optical beamformer concept for a PAA receiver system is proposed that can operate squint-free within a wide frequency band, without requiring tunable lasers. It is based on coherent optical combining in an optical beamforming network (OBFN) using cascades of optical ring resonators (ORRs) [21]–[36] as tunable delay elements. A dedicated system architecture for performing the electro-optical (E/O) and opto-electrical (O/E) conversions is proposed that relaxes the requirements on the complexity of the OBFN. It will be illustrated that the proposed concept has potential for full integration of the optical beamformer.

A typical application of the presented beamformer concept is a broadband transceiver employing a PAA with a large number of elements and stringent requirements on the beam angle accuracy, for instance for radar or satellite communications. An example of such an application is an airborne satellite receiver, which can provide in-flight connectivity for flight crew information, and live TV and high-speed Internet connectivity for passengers. Novel technology for such a receiver has recently been developed within the framework of the SMart Antenna systems for Radio Transceivers (SMART) project [31], [32], by a Dutch consortium consisting of the Dutch National Aerospace Laboratory NLR, Cyner Substrates, the University of Twente, and LioniX B.V. It is based on a non-planar PAA (conformal to

the aircraft fuselage) consisting of novel broadband K_u-band stacked patch AEs, and a broadband optical beamformer employing ORRs, integrated in CMOS-compatible waveguide technology [5]. The design of the PAA and the beamformer involves several challenges:

- The power received from the satellite will be relatively low. Hence, the complete antenna system should have a high gain and low noise temperature in order to achieve satisfactory carrier-to-noise ratio (CNR), which requires the PAA to consist of many AEs (more than 1000);
- The difference in receive angles from different K_u-band satellites can be as low as 2 degrees, which requires a very narrow antenna beam with a very high angle accuracy;
- In contrast to the situation in for instance a vehicle, where only one receiver needs to demodulate a single (relatively narrowband) television channel at a time (which could for example be done by means of digital beamforming), the airline passengers should be able to choose television channels individually. This implies that the PAA should in this case be able to accommodate the entire K_u band at once (i.e., 10.7–12.75 GHz).

For the beamformer this implies that it should have many inputs, and that it should be able to accommodate relatively large delays, a large bandwidth, and seamless tunability. In Part I of this paper it is explained how this can be achieved by means of an ORR-based optical beamformer. Although the theory will be presented in such a way that it is generally applicable, the practical numerical examples will be based on the application that is studied in the SMART project, i.e., satellite television reception. In Part II [36] the realization and testing of an experimental ORR-based optical beamformer setup will be described, including the design and fabrication of the optical devices. This beamformer setup was realized as a part of an an experimental system demonstrator that was developed in the SMART project [32].

Part I is organized as follows. In the next section, the theoretical principles of ORR-based OBFNs will be summarized. After that, the design of the modulation and detection scheme will be be outlined in Section III. In Section IV the impact of the proposed optical beamformer on the noise performance of the receiver is analyzed. Both the design and the performance analysis are illustrated by a numerical example in Section V. The paper ends with conclusions in Section VI.

II. PRINCIPLES OF RING RESONATOR-BASED OPTICAL BEAMFORMING NETWORKS

A. Optical Ring Resonator-Based Delay Elements

When an optical carrier is modulated by an RF signal, propagates through an optical waveguide, and is converted to the electrical domain by an optical detector, the effective time delay to the RF signal is determined by the group delay of the optical waveguide. This group delay can be made tunable by putting an ORR parallel to the waveguide [21]–[25], as illustrated in the inset of Fig. 1. The resulting structure has a time-discrete impulse response, and—as a result—a periodic transfer function. The period is called free spectral range (FSR), and is equal to the inverse of the round-trip time τ_r of the ring. When the losses in
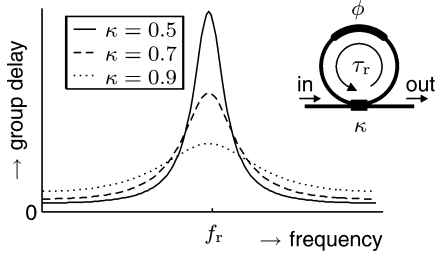
Fig. 1. Theoretical group delay response of the ring resonator-based delay element shown at the inset, for different values of the power coupling coefficient κ. The optical ring resonator (ORR) has a round-trip time τ_{r}, a round-trip phase shift ϕ and a resonance frequency f_{r}.

Fig. 2. Theoretical group delay response of three cascaded ORR sections (shown at the inset), with resonance frequencies f_i. The dashed curves denote the group delay responses of the individual sections, whereas the solid curve denotes their sum. In this case the round-trip phase shifts ϕ_i and power coupling coefficients κ_i of the individual sections are tuned such that the total resulting group delay response is flattened.

the waveguide and in the ring can be neglected, all optical power entering at the input port will eventually arrive at the output port, so the magnitude of the transfer function will be one. The group delay response will also be periodic, with the same FSR, and can be found by differentiating the phase response with respect to frequency, resulting in [21]–[24]

$$\tau_{\mathrm{g}}(f) = \frac{\kappa \tau_{\mathrm{r}}}{2 - \kappa - 2\sqrt{1-\kappa}\cos(2\pi f \tau_{\mathrm{r}} + \phi)} \qquad (1)$$

where ϕ is the round-trip phase shift of the ring, and κ is the power coupling coefficient between the waveguide and the ring. Each period of the group delay response is a symmetric, bell-shaped function of frequency, centered around the resonance frequency f_{r} of the ring. This resonance frequency can be varied by tuning the round-trip phase shift ϕ of the ring, and the maximum delay value can be varied by tuning the power coupling coefficient κ between the waveguide and the ring. This is illustrated in Fig. 1, where one period of the group delay response is plotted for a fixed value of ϕ and three different values of κ. The value of ϕ should be tuned such that the bell shape is aligned with the spectrum of the modulated optical signal, and κ should be tuned such that the desired delay value is achieved in the peak. The value of ϕ can be tuned by means of an optical phase shifter, and the value of κ can be tuned by means of a symmetric Mach-Zehnder interferometer (MZI) with an optical phase shifter in one of its arms. Optical phase shifters can be implemented for instance using the electo-optic or thermo-optic effect.

The peak value of the delay is more or less inversely proportional to the peak width. This is because the area underneath the delay curve in one period is equal to $1/(2\pi)$ times the phase transition within one period. Since this phase transition is always equal to 2π, the area under the group delay response in one period is always equal to one. Hence, when the peak delay value of the ORR is increased, the bandwidth decreases, revealing an inherent tradeoff of the ORR-based delay element [21]–[25]. As a result, a single ORR might not provide enough delay and bandwidth for a broadband RF signal.

B. Multi-Ring Delay Elements

The bandwidth of an ORR-based delay element can be enhanced by cascading several ORR sections [21], [22], [24], [25], as illustrated in the inset of Fig. 2. The total group delay response of this cascade can be found by summing the individual
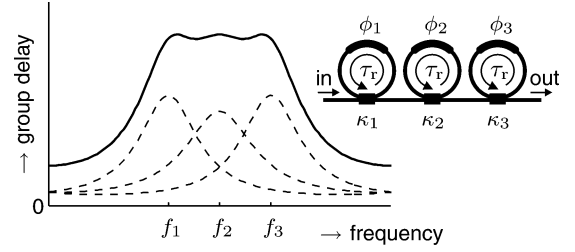
group delay responses of the constituting sections. Hence, a flattened group delay response can be obtained by tuning the individual sections to different resonance frequencies, and slightly different peak delay values, as illustrated in Fig. 2. This flattened part will have a ripple, which may cause distortion to the RF signal that is modulated onto the optical carrier. However, this ripple can be made arbitrarily small by either squeezing the resonance frequencies closer to each other (although that would reduce the bandwidth), or by adding more rings to the cascade (but that will increase the complexity of the delay element). Hence, multi-ring delay elements show an inherent trade-off between peak delay, bandwidth, delay ripple, and number of rings [21], [22], [24], [25]. In other words, for a specified maximum ripple that can be tolerated, the complexity of the delay elements increases with increasing values of the required maximum delay and the required optical bandwidth. We will explain how these can be minimized in Section II-C and Section III, respectively.

In [25] we have presented group delay measurements on a three-ring optical delay device, showing good agreement with the theory. This device was realized in CMOS-compatible optical waveguide technology [5], using thermal tuning by means of chromium heaters.

C. Optical Beamforming Network Structure

A full OBFN is obtained by combining the ORR-based delay elements with tunable optical signal processing circuitry (power splitters or combiners). Integrating this into one device rather than grouping multiple optical devices together, has several advantages such as compact size, lower loss, and reduced assembly costs. Moreover, it enables the optical signals to be combined coherently when the OBFN is operated in receive mode. This implies that the E/O and O/E conversions can be performed by means of only one laser and detector (as will be discussed in Section III), and it increases the efficiency from the point of view of optical power.

An example of a 4×1 OBFN is shown in Fig. 3. It is based on a binary tree topology, consisting of two stages, four inputs, three tunable optical combiners, and one output. In this particular case a total of four rings is involved. The rationale for using such a topology is that, for a linear PAA, increasing delay tuning ranges are required for the four possible paths through the OBFN, where the upper path (from Input 1 to the output) is
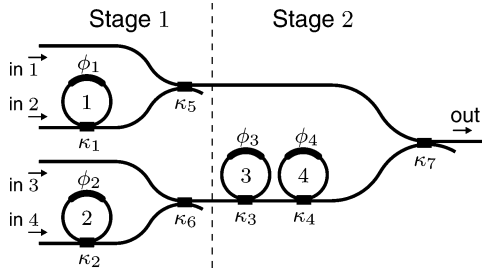
Fig. 3. Binary tree-based 4×1 optical beamforming network (OBFN) consisting of four ORRs and three combiners.
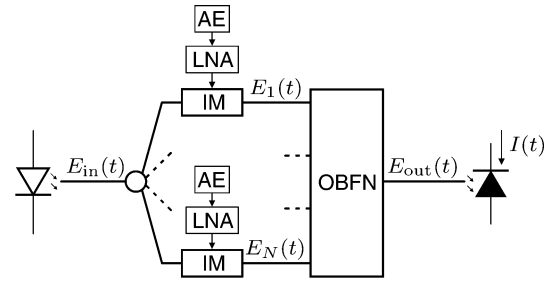

Fig. 4. Beamformer scheme with N inputs, using optical intensity modulation (IM) and direct optical detection. (AE = antenna element, LNA = low-noise amplifier, OBFN = optical beamforming network).

considered as the reference path. On the other hand, two neighbouring AEs require similar delay values, so the correponding paths in the OBFN have only a small difference in delay. From the considerations in Section II-B it follows that this difference can therefore be tuned by a low number of rings in the first stage, whereas the (larger) common delay can be tuned by a common delay element (requiring more rings) in a common part of these paths, in the next stage. This can be generalized to larger OBFNs, for example 8×1, 16×1, etcetera. This approach will result in a minimum total required number of rings for the complete OBFN. The total number depends on

- the required delay tuning range per delay element (which is determined by the PAA geometry and the maximum scan angle);
- the required delay ripple (or, for example, the accuracy of the corresponding phase response);
- the required optical bandwidth.

In this paper we will not go into further detail on the required delay values and their accuracy, but we will focus on approaches to build up the system around the OBFN in such a way that the required optical bandwidth is minimized. This will be discussed in Section III.

In [26], [27] we presented group delay measurements on a single-chip realization of such a 4×1 ORR-based OBFN, fabricated in CMOS-compatible waveguide technology. Later we extended these to an 8×1 OBFN [28]–[32]. We also presented time domain measurements on a 2×1 OBFN [33], and coherent combining of multiple input signals [32], [34].

III. DESIGN OF THE OPTICAL MODULATION AND DETECTION SCHEME

Several considerations have to be made when choosing the way in which the optical signals entering the OBFN are to be modulated by the AE signals, and this will have consequences for the way in which the optical signal should be detected after optical beamforming. As discussed in Section II, an important criterion is that the bandwidth of the modulated optical signals should be minimized, in order to minimize the required complexity of the OBFN. Moreover, the optical beamformer should be designed in such a way that its impact on the performance of the full receiver system (in terms of dynamic range) is kept within acceptable bounds. This implies that the noise, loss, and non-linear distortion in the optical modulation and detection should be minimized.

A. Common Laser and Detector

A first consequence of the bandwidth requirement is that the optical sources should be narrowband, i.e., the bandwidths of the modulated optical signals should be determined by the inherent spectral broadening due to the modulation, and not by the bandwidth of the source signal itself. In other words, the bandwidth of the source signal should be much smaller than the bandwidth of the modulating signals.

The most straightforward way of performing the E/O conversion would then be to use directly modulated lasers, but this has three important drawbacks. First of all, directly modulating a laser will cause frequency chirping [37], resulting in spectral broadening. Secondly, direct modulation techniques suffer from a limited dynamic range due to the elevated noise and distortion levels at high frequencies [38], [39]. Therefore, E/O conversion should be performed by externally modulating continuous-wave (CW) light. A third problem is that using a separate laser for each individual AE signal would lead to incoherent optical combining, resulting in optical beat interference (OBI) noise. The bandwidth of this noise would be in the same order of magnitude as the source signal's bandwidth. As discussed before, this bandwidth should be as low as possible, so the OBI noise would be completely in the signal band. As a result, it would not be possible to filter out the OBI noise, so it would completely corrupt the output signal of the beamformer. This is prevented when a common CW laser and coherent optical combining is used. This requires the coherence time of the source to be much larger than the maximum difference between the group delays of the different beamformer paths, in order to maintain correlation between the optical phases. Moreover, the signals that are combined have to be synchronized in optical phase; this will be further discussed in Section III-E.

B. Optical Intensity Modulation and Direct Optical Detection

First we consider the technique that should be used for the external modulation. The most straightforward choice would be to use intensity modulation (IM)—for instance by means of electro-absorption modulators (EAMs) or Mach-Zehnder modulators (MZMs)—and direct optical detection, using a photodiode. This would result in a scheme as shown in Fig. 4.

As the optical intensity is proportional to the square of the optical field, even perfectly linear IM would result in an optical field that has a square-root dependence on the modulating
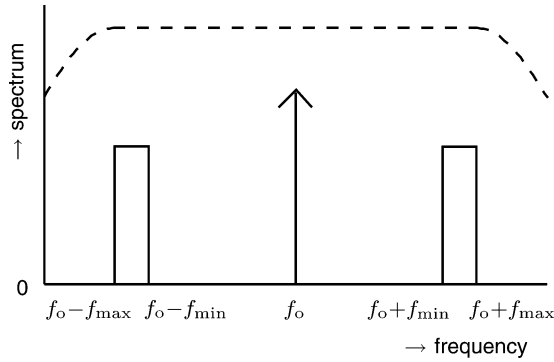
Fig. 5. Spectrum of the modulated optical signal (solid line) in case of optical intensity modulation by an RF bandpass signal, and corresponding desired group delay response (dashed line) of a delay element in the OBFN. f_o denotes the optical carrier frequency, and f_{min} and f_{max} denote the lower and upper bound of the frequency range of the modulating RF signal, respectively.
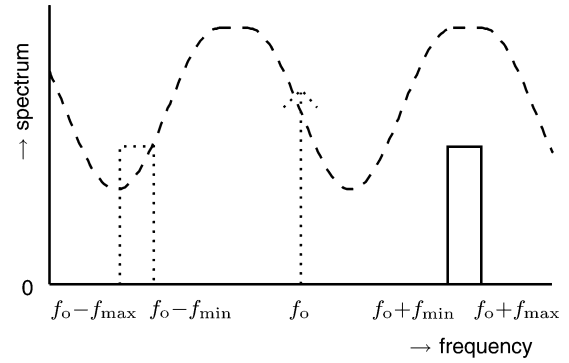

Fig. 6. Spectrum of the modulated optical signal (solid line) in case of optical single-sideband suppressed-carrier (SSB-SC) modulation by an RF bandpass signal (the suppressed sideband and optical carrier are represented by the dotted line), and corresponding desired group delay response (dashed line) of a delay element in the OBFN.

signal. As a result, the optical spectrum at the output of the modulator consists of the optical carrier line and an infinite number of sidebands, where the number of significant sidebands increases with increasing modulation depth. In order to keep the required complexity and the linear distortion in the OBFN to a minimum, the modulation index should be such that only the first order sidebands are significant, and the OBFN should be designed so as to provide a flat group delay response covering the optical carrier and the first order sidebands. This is illustrated in Fig. 5. As a result, the minimum optical bandwidth required to perform optical beamforming in case of IM is equal to twice the maximum frequency of the modulating RF signal. Especially in case of high-frequency PAAs with large diameters, this will result in an excessively complex OBFN. Moreover, large optical bandwidths require a large FSR of the ORRs, which corresponds to a low round-trip time and hence a small physical size. This may introduce problems with the realizability of the corresponding optical chips.

In the numerical example that will be presented in Section V, it will be shown that a PAA for receiving K_u-band satellite signals (10.7–12.75 GHz) requires the beamformer to provide delays up to roughly 4.3 ns. When IM is performed, the bandwidth of the modulated optical signals will be twice the maximum RF frequency. As a result, in this case the delay elements in the OBFN would be required to provide delays in the order of 4.3 ns over an optical bandwidth of 25.5 GHz, which corresponds to a (linear) phase transition of 110 times 2π. Since the flat part of the group delay response should be within one period of the ORRs, and one ORR can provide a phase transition of at most 2π within one period (see Section II-B), it follows that at least 110 ORRs would be required to achieve this. (In practice this number will be even higher, because no delay ripple was incorporated in this lower bound.) For practical PAAs (with hundreds up till thousands of AEs), several thousands of ORRs would be required in the OBFN. This is not practical, not only because of the required optical chip area (tens to hundreds of wafers), but especially because of the excessive wiring to all the tuning elements, and immense complexity of the tuning electronics. Moreover, the FSR of the ORRs would need to be more than 25.5 GHz. This would be a problem for the technology in which

our devices were fabricated [5], which can provide a maximum FSR in the order of 15 GHz; this is further considered in Part II [36].

C. Optical SSB-SC Modulation and Balanced Coherent Optical Detection

The required complexity and FSR of the OBFN can be reduced by lowering the bandwidths of the modulated optical signals at its inputs. Looking at Fig. 5 it should be noted that the two sidebands of the intensity-modulated optical signal in fact carry the same information, while the optical carrier is only required for O/E conversion. Hence, the required optical bandwidth of the OBFN is minimized by performing optical single-sideband suppressed-carrier (SSB-SC) modulation instead of optical IM. This results in an optical spectrum as shown in Fig. 6. The dotted line represents the suppressed sideband and optical carrier, and the solid line represents the remaining sideband. The dashed line represents the shape of a possible group delay response. It illustrates that both the required optical bandwidth and the FSR of the OBFN can be significantly reduced with respect to the the situation with IM, shown in Fig. 5. For example, in the case of the satellite receiver mentioned before, the required optical bandwidth and FSR are reduced by more than 90%.

Note that removing the optical carrier is essential here. This is related to the fact that the phase relation between the optical carrier and the remaining sideband is lost when the group delay response is only optimized for the sideband frequency range. Hence, when the delayed optical SSB signals are combined such that the sidebands add up in phase, the optical carriers from the different branches might not add up in phase. Correcting this would significantly increase the required bandwidth of the OBFN, and hence the number of ORRs.

In order to convert the delayed and combined optical SSB-SC signals back to the electrical domain, the optical carrier needs to be re-inserted, but this should be done *after* the combining. It can be done by routing the unmodulated optical carrier around the OBFN and combine it with the SSB-SC-modulated output signal of the OBFN by means of a directional coupler, as illustrated in Fig. 7. Optical detection should preferably be done
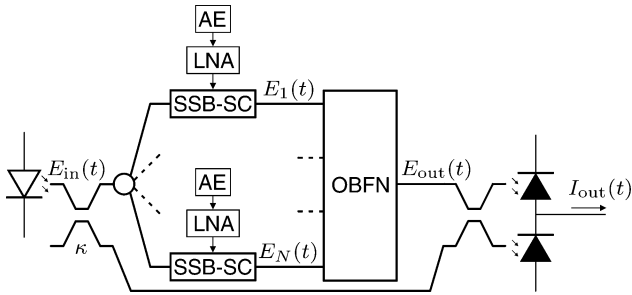
Fig. 7. Beamformer scheme with N inputs, using optical single-sideband suppressed-carrier (SSB-SC) modulation and balanced optical detection.
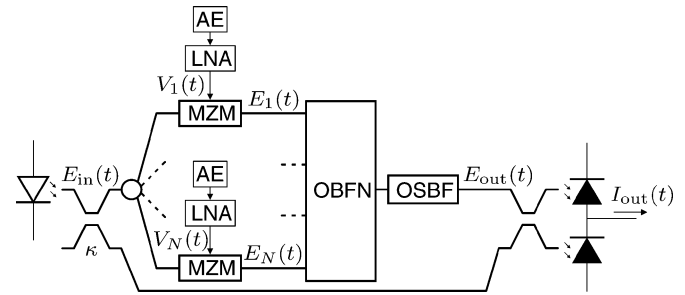

Fig. 8. Beamformer scheme with N inputs, in which the optical SSB-SC modulation is implemented by means of Mach-Zehnder modulators (MZMs) and a common optical sideband filter (OSBF).

using a balanced photodiode pair, as this considerably reduces the effect of relative intensity noise (RIN) [40].

An additional advantage of this scheme when compared to the scheme with IM and direct detection (Fig. 4) is that the phases of the RF signals that are combined can be tuned directly by tuning the optical phases of the corresponding paths in the optical beamformer. This is useful when the RF signals are down-converted before they are fed into the optical modulators, in order to reduce the bandwidth requirements of the optical modulators and detectors. Down conversion can be done by means of mixers, filters, and a common local oscillator (LO) signal. The latter is required in order to maintain correlation between the down-converted signals. Normally this would also involve a correction of the LO phase for each beamformer path, but in this case this correction can be done in the optical domain instead.

D. Implementation of Optical SSB-SC Modulation

The next design step is the choice for a suitable implementation form of the optical SSB-SC modulation. Several techniques are known for implementing optical SSB modulation. These can be divided into three categories:

1) Filter-Based Techniques: the most straightforward way of achieving optical SSB-SC modulation is to perform optical IM, and filter out the optical carrier and one of the sidebands by means of an optical sideband filter (OSBF) [41];

2) Optical Heterodyning Techniques: these rely on a combination of two lasers with an optical frequency difference that corresponds to the desired RF frequency [7]. One of the two optical carriers is first modulated with baseband data, so that mixing it with the unmodulated optical carrier results in a modulated RF signal. This technique is not applicable in our case, however, as the input signals to the modulators are already at RF; it would be more useful in cases where the RF signal is yet to be generated, for example in optical beamformers for phased-array transmit antennas. Therefore it is not further considered here;

3) Techniques Based on the Phase-Shift Method: these techniques are based on the classical SSB generation technique, where two quadrature carriers are modulated by a modulating signal and its Hilbert transform, respectively. Several optical implementation forms are known, amongst others based on a dual-electrode MZM [42], hybrid amplitude and phase modulation [43], two parallel MZMs [44], or a Sagnac loop with a unidirectional [45] or bidirectional [46] travelling-wave MZM. The double MZM seems to be the only scheme that can

support multi-octave SSB modulation with carrier suppression. (Sub-octave modulation can be a prohibitive restriction in some systems, for example when frequency down conversion is performed prior to modulation, as we did in our experimental setup [36].) However, it has the disadvantage that it requires two MZMs per AE.

The most attractive way of performing SSB-SC modulation in this particular application (see Fig. 7) is by means of IM and optical sideband filtering. It requires only one laser, and one intensity modulator per AE. The OSBFs could be put directly after the intensity modulator, but then every AE would require its own OSBF. However, since the OSBF and OBFN are both linear devices, their order can be reversed, so that only one common OSBF is required. MZMs are used as intensity modulators, as they are more linear than EAMs. This results in the system architecture that is shown in Fig. 8.

When the MZMs are operated anti-symmetrically (in push-pull mode), and properly biased, they will modulate chirp-free, and inherently suppress the optical carrier [47]. This will relax the slope requirements on the OSBF characteristic. Since the OSBF is placed after the OBFN, its phase response is not critical, as long as dispersion in the filter passband does not distort the RF signal. A relatively simple OSBF implementation that provides broad, flattened passbands and stopbands is an MZI with an ORR in one of its arms [48]. Since such an OSBF consists of similar building blocks as the OBFN (ORRs and directional couplers), both the OBFN and the OSBF can be integrated on the same chip. In [29]–[32] we presented magnitude response measurements on a chip in which such an OSBF was integrated together with a 4×1 OBFN. In [32], [34], [35] these results were extended to demonstrate that the filter successfully suppresses the undesired sideband, and that—when the OBFN is also properly tuned—the RF-to-RF transfer from modulator input to detector output indeed has a linear phase response in the RF range of interest, according to the desired delay. In Part II of this paper [36] measurements will be presented on an optical chip that was specifically designed for satellite television reception.

E. Optical Phase Synchronization

An essential property of the OBFN is that the optical input signals are combined *in phase*, as far as the contributions corresponding to AE input signals from the *desired direction* are concerned. This not only requires the ORR-based delay elements

to compensate for differences in arrival time, but also involves synchronization on the optical wavelength level. This was an issue in our experimental setup, because so far, in our implementation, only the OBFN, OSBF and carrier re-insertion coupler have been integrated on chip [36]. The splitting and modulation were done by means of fiber-based commercial off-the-shelve components, rendering the optical phase in which the signals are combined very sensitive to changes in temperature and mechanical stress, and to mechanical vibrations. Therefore, special measures are required to stabilize the input-output behavior of the beamformer. Basically two approaches can be taken.

A first approach is to use a feedback loop from the output signal to phase shifters in the OBFN paths. This could be based on the total power of the desired signal, which should be maximized. Drawbacks of this feedback criterion are the complicated relation between the output power and all the phase offsets—which hampers agile phase synchronization—and the fact that this approach might not result in proper phase-locking when interferers are present. A possible solution could be to use a frequency dithering scheme, as proposed within the framework of coherent optical code-division multiple access (OCDMA) techniques [49], but this has the disadvantage that it requires a unique oscillator for each beamformer input, which considerably complicates the feeding circuit.

A second approach is to stabilize the entire system in temperature. In our fiber-based laboratory setup this was far from straightforward, and only effective for synchronization during a few minutes (see [36] for more details). In the envisioned future implementation of the beamformer, however, the complete optical circuit—i.e., all parts between the laser and the photodetectors, including the modulators—is expected to be integrated on a single chip (or at least in one package). Such a chip can be stabilized to a pre-defined temperature with an accuracy smaller than 0.01 K, with local and temporal variations even much smaller than that. To show that this is sufficient to stabilize the phases of the combined signals, we analyze the effect of an ambient temperature change ΔT on the phase differences between the paths. Temperature changes affect the effective index of the waveguide. If we assume that the paths in the beamformer chip have equal physical lengths (which is in fact the case in the chip that we demonstrate in [36]), the resulting phase differences are mainly determined by the changes in phase transfer of the ORR-based delay elements. These changes are in turn mainly determined by variations in the round-trip phase shift $\Delta\phi$ of the ORRs, which are given by

$$\Delta\phi \approx 2\pi \frac{L}{\lambda_0} \frac{\mathrm{d}N_\mathrm{e}}{\mathrm{d}T} \Delta T \tag{2}$$

where L is the circumference of the ring, λ_0 is the optical wavelength, and $\mathrm{d}N_\mathrm{e}/\mathrm{d}T$ is the derivative of the effective index of the waveguide with respect to temperature. (Variations in the coupling coefficients κ are neglected here, because the value of κ is assumed to be tuned by means of a symmetric MZI, and the phase difference between two paths in a symmetric MZI is much less sensitive to temperature variations than the round-trip phase shift in an ORR.) Since the FSR of an ORR can be expressed as $\mathrm{FSR} = c_0/(N_\mathrm{g}L)$, where N_g is the effective group index of the

waveguide, such change in round-trip phase $\Delta\phi$ will result in a (horizontal) frequency shift of the phase response by a value

$$\Delta f = \frac{\Delta\phi}{2\pi}\mathrm{FSR} = \frac{c_0}{\lambda_0 N_\mathrm{g}} \frac{\mathrm{d}N_\mathrm{e}}{\mathrm{d}T} \Delta T. \tag{3}$$

When the ORRs are properly tuned, the phase response of each delay element is linear with frequency, with a slope that is equal to $-2\pi\tau_\mathrm{g}$, where τ_g is the group delay to which the delay element is tuned. The shift in frequency will hence result in a phase change

$$\Delta\Phi = 2\pi\tau_\mathrm{g}\Delta f \tag{4}$$

$$= 2\pi \frac{c_0\tau_\mathrm{g}}{\lambda_0 N_\mathrm{g}} \frac{\mathrm{d}N_\mathrm{e}}{\mathrm{d}T} \Delta T. \tag{5}$$

Assuming a maximum group delay difference between the paths of 4.3 ns (see the numerical example in Section V), an effective group index of 1.55, an optical wavelength of 1550 nm, and $\mathrm{d}N_\mathrm{e}/\mathrm{d}T = 10^{-5}\ \mathrm{K}^{-1}$, we find that temperature fluctuations below 0.01 K result in phase fluctuations below $\pi/10$ radians, which should be considered acceptable for this application.

Frequency fluctuations of the laser have a similar effect as the frequency shift in the phase response, so it follows from (4) that fluctuations below 10 MHz (which are achievable using temperature control) will also result in phase errors below $\pi/10$ radians.

Hence it is expected that the optical phase differences between the different paths in the chip will be sufficiently stable, so that optical phase synchronization only requires an initial calibration, and possibly on-the-fly phase corrections based on the remaining settings of the OBFN.

If we assume that the OSBF is realized as an asymmetric MZI with an ORR in one of its arms, as we did in the chip that is presented in Part II of this paper [36], a similar calculation can be done to show that the transfer function of the OSBF (also given in [36]) is even much less sensitive to temperature changes and laser drift than the OBFN.

IV. PERFORMANCE ANALYSIS

An important consideration in the design of the beamformer is the impact that it will have on the performance of the full receiver system, in terms of noise and/or distortion. In order to analyze this, we first require a framework to describe this impact, in terms of system gain, system noise temperature, and the effect of non-linearities. This framework is based on an equivalent two-port model of the complete receiver system—including AEs and LNAs—and is further described in Section IV-A. Then, in Section IV-B, the relation between the input voltages and the output current of the beamformer is studied. This relation is used to calculate the system gain and noise temperature, in Sections IV-C and IV-D, respectively. The impact of non-linearities in the beamformer is studied in Section IV-E. In Section IV-F an expression is derived for the CNR at the output of the beamformer.

A. Analysis Framework

The PAA with optical beamformer is essentially an analog optical signal processor, that can be described as a multiport
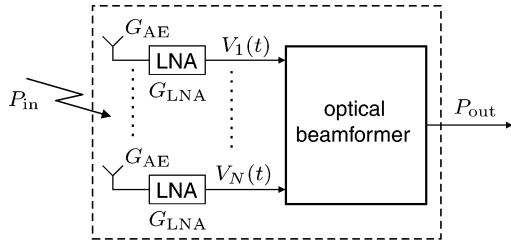
Fig. 9.   Multiport RF system model.

Fig. 10.   Equivalent two-port system model.

RF component. A system model is shown in Fig. 9. The system has N input branches, and each branch consists of an AE with gain G_{AE}, and a low-noise amplifier (LNA) with gain G_{LNA} and effective input noise temperature T_{LNA}. The input power P_{in} is defined as the power that a lossless, passive, and isotropic antenna would receive. P_{out} is the output power of the beamformer. Note that G_{AE} represents the gain per AE *in the array*, i.e., it may differ from the gain of a separated AE. Its value generally depends on the array structure, AE spacing, beam direction, and possible mutual coupling between the AEs. This is not considered in further detail here. For simplicity, edge effects are neglected, so it is assumed that all the AEs have the same gain G_{AE}. (In practice this could be achieved by adding dummy AEs at the edges of the array.)

An approach for describing such a multiport in terms of gain and noise figure was introduced in [50]. Our approach will be slightly different, however, for the following four reasons:

1) The description in [50] is limited to the description of the optical beamformer itself, whereas we prefer a description that provides a better understanding of the full receiver system in which the beamformer is applied, i.e., also describing the AEs, the LNAs, and the actual signals that are received;

2) The beamformer types that are considered in [50] are fundamentally different from ours, both regarding E/O and O/E conversion (IM and direct detection, rather than optical SSB-SC modulation and balanced coherent detection), and the way in which the optical signals are combined (coherent optical combining is not considered in [50]);

3) The effect of non-linearities is not studied in [50]. However, as we will show here, the non-linearity in the MZMs will affect the design and eventual performance of the system;

4) Amplitude tapering is not considered in [50], whereas we will show that it can easily be incorporated in the general description.

For a performance analysis on system level, the multiport system is reduced to an equivalent two-port RF component, as shown in Fig. 10 [51]. It consists of a single equivalent antenna with gain (or directivity) G_{a} and the same input power P_{in} as the multiport system, and an equivalent receiver with gain G_{rec} and the same output power P_{out} as the multiport system. The equivalent antenna is considered passive and lossless, and includes the antenna patterns of the individual AEs, as well as the gain from coherent combining and possible amplitude tapering. The equivalent receiver contains the so-called uncorrelated
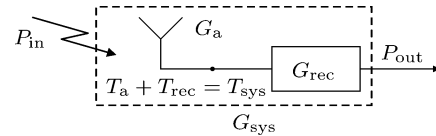
receiver gain, which describes the system as if all its inputs were excited by uncorrelated sources of equal power. Note that the signal level at the output of the equivalent antenna does not correspond with any signal level in the original multiport system.

The equivalent system is described in terms of a power gain $G_{\mathrm{sys}} = G_{\mathrm{a}}G_{\mathrm{rec}}$, and effective system noise temperature T_{sys} at the output terminals of the equivalent antenna. The latter describes the noise that is present in the system. It is the sum of antenna noise temperature T_{a}, which models the sky noise and antenna noise, and receiver noise temperature T_{rec}, which models the noise from the RF front-ends (LNAs) and the optical beamformer. In order to express these parameters in terms of the parameters of the components that build up the complete system, we first need to find the relation between the input and output signals of the optical beamformer in Fig. 9.

B. Input-Output Relation of the Optical Beamformer

We derive this relation by analyzing the beamformer circuit in Fig. 8 from left to right, i.e., we start by modeling the laser output and see how it is processed as it propagates through the beamformer circuit. Although the output field of a laser generally suffers from phase noise and RIN, these effects are assumed to be negligible in the analysis. RIN is neglected as it is largely suppressed in the balanced detector [40], and phase noise is ignored because it is assumed that the coherence time of the laser is much larger than all the differences in group delay between the different paths through the optical circuit. Therefore the (complex) analytical signal representation of the optical field that is coupled into the optical circuit is denoted by

$$E_{\mathrm{in}}(t) = \sqrt{\frac{2P_{\mathrm{o}}}{L_{\mathrm{lc}}}} \exp(\mathrm{j}2\pi f_{\mathrm{o}}t) \qquad (6)$$

where P_{o} is the output power of the laser, f_{o} is the optical carrier frequency, and L_{lc} is the coupling loss between the laser and the circuit. The transfer matrix of a 2×2 directional coupler is given by

$$\mathbf{H}_{2\times 2} = \begin{bmatrix} \sqrt{1-\kappa} & \mathrm{j}\sqrt{\kappa} \\ \mathrm{j}\sqrt{\kappa} & \sqrt{1-\kappa} \end{bmatrix} \qquad (7)$$

where κ is the power coupling coefficient. As a result, a fraction $1 - \kappa$ of the input power is assumed to enter the splitter in front of the modulators, whereas a fraction κ is directly fed to the carrier re-insertion coupler. The $1 \times N$ splitter in front of the modulators may be non-uniform and tunable, in order to enable amplitude tapering. When the splitting loss to the nth branch of the beamformer is denoted by $L_{\mathrm{s},n}$, the optical field entering the nth modulator can be written as

$$E_{\mathrm{in},n}(t) = \sqrt{\frac{2(1-\kappa)P_{\mathrm{o}}}{L_{\mathrm{lc}}L_{\mathrm{s},n}}} \exp(\mathrm{j}2\pi f_{\mathrm{o}}t). \qquad (8)$$

Now suppose that the MZMs are operated in push-pull mode, and biased in the minimum transmission point. Then the optical fields at the input and output of the nth modulator are related by [47]

$$E_n(t) = \frac{1}{\sqrt{L_{\mathrm{m}}}} E_{\mathrm{in},n}(t) \sin\left(\frac{\pi V_n(t)}{2V_\pi}\right) \qquad (9)$$

where L_{m}, $V_n(t)$, and V_π are the excess loss, RF input voltage, and RF half-wave voltage of the modulator, respectively. $V_n(t)$ consists of a desired signal, possible interfering signals, and noise, and is assumed to be band-limited around some carrier frequency f_{RF}. It can hence be written in the amplitude and phase form

$$V_n(t) = \hat{V}_n(t) \cos(2\pi f_{\mathrm{RF}} t + \psi_n(t)). \qquad (10)$$

When (8) and (10) are substituted in (9), and it is (for the time being) assumed that $\hat{V}_n(t)$ is sufficiently small so that a first order approximation can be used for the sine function, then we can approximate the optical fields entering the OBFN as

$$\begin{aligned} E_n(t) &\approx \frac{\pi}{2V_\pi\sqrt{L_{\mathrm{m}}}} E_{\mathrm{in},n}(t) V_n(t) \\ &= \frac{\pi}{4V_\pi}\sqrt{\frac{2(1-\kappa)P_{\mathrm{o}}}{L_{\mathrm{lc}}L_{\mathrm{s},n}L_{\mathrm{m}}}}\hat{V}_n(t) \\ &\quad \cdot [\exp(\mathrm{j}2\pi(f_{\mathrm{o}}+f_{\mathrm{RF}})t + \mathrm{j}\psi_n(t)) \\ &\quad + \exp(\mathrm{j}2\pi(f_{\mathrm{o}}-f_{\mathrm{RF}})t - \mathrm{j}\psi_n(t))]. \end{aligned} \qquad (11)$$

The two terms between the square brackets correspond to the upper and lower sideband in Fig. 6, respectively.

In the OBFN the output signals are delayed and combined. Suppose that the ORR-based delay elements in the OBFN are tuned to have a flat group delay response in the frequency range of the upper sideband of (11). When the group delay in the nth path is denoted by τ_n, the group delay ripple is neglected, the total propagation loss in the corresponding delay elements is denoted by $L_{\mathrm{d},n}$, and the combining loss is denoted by $L_{\mathrm{c},n}$, then the transfer function from Input n to the output of the OBFN in the frequency range of the upper sideband can be written as

$$H_n(f) = \frac{\exp(\mathrm{j}\theta_n - \mathrm{j}2\pi(f-f_{\mathrm{o}}-f_{\mathrm{RF}})\tau_n)}{\sqrt{L_{\mathrm{d},n}L_{\mathrm{c},n}}} \qquad (12)$$

where θ_n denotes the optical phase shift at frequency $f_{\mathrm{o}}+f_{\mathrm{RF}}$ in the nth path. For the OSBF it is assumed that it fully suppresses the lower sideband, and fully passes the upper sideband, without significant distortion. When the passband loss is denoted by L_{f}, then the optical field at the output of the OSBF follows from (11) and (12) as

$$\begin{aligned} E_{\mathrm{out}}(t) &= \frac{\pi}{4V_\pi}\sqrt{\frac{2(1-\kappa)P_{\mathrm{o}}}{L_{\mathrm{lc}}L_{\mathrm{m}}L_{\mathrm{f}}}} \sum_n \frac{\hat{V}_n(t-\tau_n)}{\sqrt{L_{\mathrm{s},n}L_{\mathrm{d},n}L_{\mathrm{c},n}}} \\ &\quad \cdot \exp(\mathrm{j}2\pi(f_{\mathrm{o}}+f_{\mathrm{RF}})t + \mathrm{j}\psi_n(t-\tau_n) + \mathrm{j}\theta_n). \end{aligned} \qquad (13)$$

The propagation losses $L_{\mathrm{d},n}$ of the delay elements are roughly proportional to their group delay responses [22], [25], and, as a result, are different for every path. This can be compensated for by properly tuning $L_{\mathrm{s},n}$ and $L_{\mathrm{c},n}$, which also enables amplitude tapering. Hence, we can write

$$\begin{aligned} E_{\mathrm{out}}(t) &= \frac{\pi}{4V_\pi}\sqrt{\frac{2(1-\kappa)P_{\mathrm{o}}}{NL_{\mathrm{lc}}L_{\mathrm{mp}}}} \sum_n a_n \hat{V}_n(t-\tau_n) \\ &\quad \cdot \exp(\mathrm{j}2\pi(f_{\mathrm{o}}+f_{\mathrm{RF}})t + \mathrm{j}\psi_n(t-\tau_n) + \mathrm{j}\theta_n) \end{aligned} \qquad (14)$$

where the passive taper coefficients

$$a_n \triangleq \sqrt{\frac{(L_{\mathrm{s},n}L_{\mathrm{d},n}L_{\mathrm{c},n})^{-1}}{\sum_m (L_{\mathrm{s},m}L_{\mathrm{d},m}L_{\mathrm{c},m})^{-1}}} \qquad (15)$$

are defined such that $\sum_n a_n^2 = 1$, and

$$L_{\mathrm{mp}} \triangleq \frac{L_{\mathrm{m}}L_{\mathrm{f}}}{N \sum_n (L_{\mathrm{s},n}L_{\mathrm{d},n}L_{\mathrm{c},n})^{-1}} \qquad (16)$$

can be considered as a measure for the total excess loss in the modulated path of the optical circuit. (Note that $L_{\mathrm{mp}} = L_{\mathrm{m}}L_{\mathrm{f}}$ when $L_{\mathrm{s},n} = L_{\mathrm{c},n} = N$ and $L_{\mathrm{d},n} = 1$.)

The carrier re-insertion coupler is assumed to be lossless and perfectly balanced, so its transfer matrix is given by (7), with $\kappa = 1/2$. The photodiodes are assumed to be identical and perfectly linear, so the relation between a photodiode current $I_{\mathrm{pd}}(t)$ and the optical field $E_{\mathrm{pd}}(t)$ at its input is given by

$$I_{\mathrm{pd}}(t) = \frac{1}{2}R_{\mathrm{pd}}|E_{\mathrm{pd}}(t)|^2 + I_{\mathrm{sn}}(t) \qquad (17)$$

where R_{pd} denotes the responsivity of the photodiode, and $I_{\mathrm{sn}}(t)$ is the shot noise current. We will get back to the latter in Section IV-D. The fields at the two inputs of the carrier re-insertion coupler are $E_{\mathrm{out}}(t)$ and $\mathrm{j}\sqrt{\kappa/L_{\mathrm{up}}}E_{\mathrm{in}}(t)$, respectively, where L_{up} is the total excess loss in the unmodulated path of the optical circuit. Assuming a coupling loss L_{cd} between the circuit and the photodetector, it follows that the output current of the balanced detector can be written as

$$\begin{aligned} I_{\mathrm{out}}(t) &= \frac{R_{\mathrm{pd}}}{2L_{\mathrm{cd}}} \left[\left| \frac{E_{\mathrm{out}}(t)}{\sqrt{2}} - \sqrt{\frac{\kappa}{2L_{\mathrm{up}}}}E_{\mathrm{in}}(t) \right|^2 \right. \\ &\quad \left. - \left| \frac{\mathrm{j}E_{\mathrm{out}}(t)}{\sqrt{2}} + \mathrm{j}\sqrt{\frac{\kappa}{2L_{\mathrm{up}}}}E_{\mathrm{in}}(t) \right|^2 \right] \\ &\quad + I_{\mathrm{sn},1}(t) - I_{\mathrm{sn},2}(t) \\ &= -\frac{R_{\mathrm{pd}}\sqrt{\kappa}}{L_{\mathrm{cd}}\sqrt{L_{\mathrm{up}}}} \mathrm{Re}\{E_{\mathrm{out}}(t)E_{\mathrm{in}}^*(t)\} + I_{\mathrm{sn,out}}(t) \end{aligned} \qquad (18)$$

where $\mathrm{Re}\{.\}$ denotes real part. Substituting (6) and (14) this becomes

$$\begin{aligned} I_{\mathrm{out}}(t) &= -\frac{\pi R_{\mathrm{pd}}P_{\mathrm{o}}}{2V_\pi L_{\mathrm{lc}}L_{\mathrm{cd}}}\sqrt{\frac{\kappa(1-\kappa)}{NL_{\mathrm{mp}}L_{\mathrm{up}}}} \sum_n a_n \hat{V}_n(t-\tau_n) \\ &\quad \cdot \cos(2\pi f_{\mathrm{RF}} t + \psi_n(t-\tau_n) + \theta_n) + I_{\mathrm{sn,out}}(t). \end{aligned} \qquad (19)$$

Now suppose that the optical phases of the signals that are combined are tuned such that $\theta_n = -2\pi f_{\mathrm{RF}}\tau_n$. It can be verified that (19) can then be simplified using (10), resulting in

$$I_{\mathrm{out}}(t) = -\frac{\pi R_{\mathrm{pd}}P_o}{2V_\pi L_{\mathrm{lc}}L_{\mathrm{cd}}}\sqrt{\frac{\kappa(1-\kappa)}{NL_{\mathrm{mp}}L_{\mathrm{up}}}}\sum_n a_n V_n(t-\tau_n) \\ +I_{\mathrm{sn,out}}(t). \quad (20)$$

The values of the delays τ_n should be chosen such that the desired terms in the delayed input voltages $V_n(t-\tau_n)$ are time-synchronized. Properly tuning the values of θ_n is then a matter of optical phase synchronization (see Section III-E).

C. Gain

In order to find expressions for the gains that were introduced in Section IV-A, we need to relate the inputs and output of the *complete receiver system* in terms of *power*. The total gain G_{sys} of the equivalent system is equal to the *coherent gain* or *signal gain* [51], i.e., the gain that the input power P_{in} in Fig. 9 sees when its contributions to the AE signals add up coherently in the beamformer. This can be derived from (20), by noting that the input power to the nth beamformer input can be expressed in terms of the PAA input power P_{in} as $G_{\mathrm{AE}}G_{\mathrm{LNA}}P_{\mathrm{in}}$, but also in terms of the modulator input voltage $V_n(t)$ as $\langle V_n^2(t)\rangle/R_{\mathrm{m}}$, where $\langle\cdot\rangle$ denotes mean value, and R_{m} is the input impedance of the MZMs. The actual output power P_{out} depends on the way in which the photodiodes are connected to the next stage of the receiver. In this case, we simply assume that there is no matching circuit, and that the output current $I_{\mathrm{out}}(t)$ is dissipated in a load impedance R_L, resulting in an output power $P_{\mathrm{out}} = \langle I_{\mathrm{out}}^2(t)\rangle R_L$. (If a resistive matching circuit were included, this would simply decrease by 6 dB.) Assuming that the input voltages $V_n(t)$ add up coherently, it now follows from (20) that the coherent gain is given by

$$G_{\mathrm{sys}} = \frac{G_{\mathrm{AE}}G_{\mathrm{LNA}}R_{\mathrm{m}}R_L(\pi R_{\mathrm{pd}}P_o)^2\kappa(1-\kappa)\eta_t}{4(V_\pi L_{\mathrm{lc}}L_{\mathrm{cd}})^2 L_{\mathrm{mp}}L_{\mathrm{up}}} \quad (21)$$

where η_t is the *taper efficiency*

$$\eta_t \triangleq \frac{1}{N}\left(\sum_n a_n\right)^2. \quad (22)$$

Note that $\eta_t = 1$ for uniform tapering.

The receiver gain G_{rec} is equivalent to the *incoherent gain* or *noise gain*, i.e., the gain that the individual input (noise) powers (at the inputs of the LNAs, so excluding G_{AE}) see when they add up incoherently in the beamformer. Using (20) this can be shown to result in

$$G_{\mathrm{rec}} = G_{\mathrm{LNA}}G_{\mathrm{OBF}} \quad (23)$$

with

$$G_{\mathrm{OBF}} = \frac{R_{\mathrm{m}}R_L(\pi R_{\mathrm{pd}}P_o)^2\kappa(1-\kappa)}{4N(V_\pi L_{\mathrm{lc}}L_{\mathrm{cd}})^2 L_{\mathrm{mp}}L_{\mathrm{up}}}. \quad (24)$$

The latter can be considered as the *intrinsic receiver gain* of the beamformer, i.e., it is the equivalent receiver gain of the beamformer excluding the LNAs. In other words, the equivalent

receiver could be modeled as a cascade of one LNA, with gain G_{LNA}, and the equivalent receiver that would be obtained if there were no LNAs, with gain G_{OBF}.

Since the total system gain can be written as $G_{\mathrm{sys}} = G_a G_{\mathrm{rec}}$ (see Fig. 10), we find for the equivalent antenna gain

$$G_a = G_{\mathrm{AE}}\eta_t N. \quad (25)$$

D. Noise

The noise at the output of the beamformer is partly caused by the antenna noise that is already present at the input, and partly by receiver noise. The effective noise temperature of the equivalent antenna is approximated by the brightness temperature of the sky T_b in the direction of the main lobe, so $T_a \approx T_b$. Using Friis' formula, the effective input noise temperature of the equivalent receiver can be written as

$$T_{\mathrm{rec}} = T_{\mathrm{LNA}} + \frac{T_{\mathrm{OBF}}}{G_{\mathrm{LNA}}} \quad (26)$$

where T_{LNA} is the effective input noise temperature of the LNAs, and T_{OBF} is the effective input noise temperature of the equivalent two-port model of the beamformer without LNAs. Hence, $T_{\mathrm{OBF}}/G_{\mathrm{LNA}}$ is the contribution to the system noise temperature due to noise in the optical beamformer. The latter is caused by thermal noise in the matching resistors in the MZMs, shot noise in the photodiodes, thermal receiver noise, RIN, and optical phase noise. Thermal noise in the matching resistors is neglected here when compared to the LNA noise; in other words, it is assumed that $G_{\mathrm{LNA}}T_{\mathrm{LNA}}$ is much larger than the temperature of the matching resistors. As explained in the beginning of Section IV-B, RIN and phase noise are also neglected in our analysis. The thermal noise generated in the optical receiver is usually quantified in terms of the root mean square (RMS) equivalent input noise current per $\sqrt{\mathrm{Hz}}$, and depends on the implementation of the receiver. If this is denoted by I_{rms}, then the power spectral density of the equivalent input noise current is equal to I_{rms}^2. The power spectral density of the shot noise current $I_{\mathrm{sn}}(t)$ in (17) follows from Schottky's formula:

$$S_{I_{\mathrm{sn}}I_{\mathrm{sn}}}(f) = e\langle I_{\mathrm{pd}}(t)\rangle = \frac{1}{2}eR_{\mathrm{pd}}\langle|E_{\mathrm{pd}}(t)|^2\rangle \quad (27)$$

where e is the electron charge ($1.6\cdot10^{-19}$ C). The power spectral density of the total shot noise current $I_{\mathrm{sn,out}}(t)$ in (18) now follows by summing the power spectral densities of the individual shot noise currents, resulting in

$$S_{I_{\mathrm{sn,out}}I_{\mathrm{sn,out}}}(f) = \frac{eR_{\mathrm{pd}}}{2L_{\mathrm{cd}}}\left\langle\left|\frac{E_{\mathrm{out}}(t)}{\sqrt{2}} - \sqrt{\frac{\kappa}{2L_{\mathrm{up}}}}E_{\mathrm{in}}(t)\right|^2 \right. \\ \left. + \left|\frac{\mathrm{j}E_{\mathrm{out}}(t)}{\sqrt{2}} + \mathrm{j}\sqrt{\frac{\kappa}{2L_{\mathrm{up}}}}E_{\mathrm{in}}(t)\right|^2\right\rangle \\ = \frac{eR_{\mathrm{pd}}}{2L_{\mathrm{cd}}}\left\langle|E_{\mathrm{out}}(t)|^2 + \frac{\kappa}{L_{\mathrm{up}}}|E_{\mathrm{in}}(t)|^2\right\rangle. \quad (28)$$

This can be evaluated by substituting (6) and (14). When $\hat{V}_n(t)$ is small, as assumed before, the first term inside the angle

brackets can be neglected. Hence it follows that the spectral density of the power that is dissipated in the load due to the thermal noise and shot noise is given by

$$S_{\text{sn+tn}}(f) = \left[\frac{e\kappa R_{\text{pd}}P_{\text{o}}}{L_{\text{lc}}L_{\text{cd}}L_{\text{up}}} + I_{\text{rms}}^2 \right] R_{\text{L}}. \tag{29}$$

By definition, this is supposed to be equal to $G_{\text{OBF}}k_{\text{B}}T_{\text{OBF}}/2$ (where k_{B} is Boltzmann's constant, $1.38 \cdot 10^{-23}$ J/K). Hence, using (24), it follows that T_{OBF} is given by

$$T_{\text{OBF}} = \frac{8NV_\pi^2 L_{\text{lc}}L_{\text{cd}}L_{\text{mp}}(e\kappa R_{\text{pd}}P_{\text{o}} + I_{\text{rms}}^2 L_{\text{lc}}L_{\text{cd}}L_{\text{up}})}{k_{\text{B}}R_{\text{m}}(\pi R_{\text{pd}}P_{\text{o}})^2\kappa(1-\kappa)}. \tag{30}$$

Preferably, the parameter values in the beamformer should be chosen in such a way that the resulting value of $T_{\text{OBF}}/G_{\text{LNA}}$ is much smaller than T_{a} and T_{LNA}. Moreover, the total receiver gain G_{rec} in (23) should be large enough to overcome noise that is generated behind the beamformer. Otherwise the performance of the complete system would be limited by the performance of the beamformer. This will be further illustrated by the numerical example in Section V.

From (30) it also follows that the choice of a suitable value for the power coupling coefficient κ of the directional coupler directly behind the laser is a trade-off. In case the thermal noise term dominates (i.e., the second term in the numerator of (30)), its effect can be minimized by maximizing the intrinsic receiver gain G_{OBF}, by setting $\kappa = 1/2$. In case the thermal noise does not dominate, the optimum value of κ is smaller than $1/2$, as the effect of shot noise (the first term in the numerator of (30)) increases with increasing value of κ. This is not considered in further detail here.

E. Compression

Apart from noise, the beamformer will also have an impact on the distortion in the receiver, because of the non-linearity in the MZMs. In theory, this will result in an upper limit to the input power that the PAA receiver can accommodate, because of the self-compression and intermodulation distortion (IMD) to the incoming signal. This can, for instance, be expressed in the intercept point and/or 1-dB compression point of the receiver. A framework for performing such an analysis was introduced in [52], and we applied it to our beamformer in [53].

In practice, however, the upper limit to the input power of the receiver is not determined by what the receiver *can* accommodate, but by the context of the receiver, i.e., there simply is an upper limit to the power that the receiver *will* receive. (For instance, the satellite receiver considered in the numerical example in Section V is assumed to receive no more than -150 dBW from the satellite.) In that case the non-linearity will pose a limit to the maximum gain that the LNAs should have.

To analyze this we need to take a closer look at the MZM characteristic in (9), which shows the non-linear relation between RF inputs $V_n(t)$ and the optical outputs $E_n(t)$. Suppose that the

input signal is written as a signal part $V_{\text{s},n}(t)$ plus a noise part $V_{\text{n},n}(t)$. We can then rewrite (9) as

$$\begin{aligned} E_n(t) = \frac{1}{\sqrt{L_{\text{m}}}} E_{\text{in},n}(t) \Bigg[&\sin\left(\frac{\pi V_{\text{s},n}(t)}{2V_\pi}\right)\cos\left(\frac{\pi V_{\text{n},n}(t)}{2V_\pi}\right) \\ &+ \cos\left(\frac{\pi V_{\text{s},n}(t)}{2V_\pi}\right)\sin\left(\frac{\pi V_{\text{n},n}(t)}{2V_\pi}\right) \Bigg]. \end{aligned} \tag{31}$$

To study the effect of non-linearities in for example analog optical links, it is common to make third order approximations for the terms containing $V_{\text{s},n}(t)$, and first order approximations for the terms containing $V_{\text{n},n}(t)$, because the power of $V_{\text{s},n}(t)$ is usually much larger than the power of $V_{\text{n},n}(t)$. This is also what we did in [53].

This is not necessarily realistic in a PAA receiver, however, since the CNR per AE might be very small. This is particularly the case for a PAA with a large number of AEs, and that is exactly the application for which this type of beamformer is suitable. In this case, it is therefore more realistic to make first order approximations only for the terms in which $V_{\text{s},n}(t)$ appears rather than $V_{\text{n},n}(t)$, resulting in

$$\begin{aligned} E_n(t) \approx \frac{1}{\sqrt{L_{\text{m}}}} E_{\text{in},n}(t) \Bigg[&\frac{\pi V_{\text{s},n}(t)}{2V_\pi}\cos\left(\frac{\pi V_{\text{n},n}(t)}{2V_\pi}\right) \\ &+ \sin\left(\frac{\pi V_{\text{n},n}(t)}{2V_\pi}\right) \Bigg] \end{aligned} \tag{32}$$

so the signal $V_{\text{s},n}(t)$ is compressed by a (random) factor $\cos(\pi V_{\text{n},n}(t)/(2V_\pi))$. In other words, the signal mainly suffers from cross-compression with the noise, rather than self-compression and IMD, irrespective of the number of sub-carriers in the desired signal. The (thermal) noise $V_{\text{n},n}(t)$ can be assumed to be Gaussian distributed with mean zero and variance

$$\sigma_{\text{n}}^2 = \langle V_{\text{n},n}^2(t) \rangle = k_{\text{B}}(T_{\text{AE}} + T_{\text{LNA}})B_{\text{LNA}}G_{\text{LNA}}R_{\text{m}} \tag{33}$$

where T_{AE} is the average antenna noise temperature that is seen by the individual AEs, which is not necessarily equal to the antenna noise temperature T_{a} that is seen by the complete PAA. B_{LNA} is the equivalent noise bandwidth of the LNA. Using the Gaussian probability density function of $V_{\text{n},n}(t)$, the mean value of the compression factor can now be calculated as

$$\left\langle \cos\left(\frac{\pi V_{\text{n},n}(t)}{2V_\pi}\right) \right\rangle = \exp\left(-\frac{\pi^2\sigma_{\text{n}}^2}{8V_\pi^2}\right). \tag{34}$$

This implies that the total system gain G_{sys} that was derived in Section IV-C is reduced by a factor

$$\Delta G = \exp\left(-\frac{\pi^2 k_{\text{B}}(T_{\text{AE}} + T_{\text{LNA}})B_{\text{LNA}}G_{\text{LNA}}R_{\text{m}}}{4V_\pi^2}\right). \tag{35}$$

By calculating the autocorrelation function of the sine term in (32), it can be proven that the noise power at the output of the beamformer due to sky noise and LNA noise is reduced by the same factor (which should not be surprising). Therefore the net effect of the non-linearity of the MZM is that both the total system gain G_{sys} and the receiver gain G_{rec} are reduced by the same factor ΔG, so the equivalent antenna gain G_{a} remains unchanged. The contributions of the sky noise and LNA noise to

the effective system noise temperature also remain unchanged. The beamformer's contribution to the system noise temperature ($T_{\mathrm{OBF}}/G_{\mathrm{LNA}}$) is increased by the inverse of ΔG, however, since its contribution to the noise power at the output remains unchanged, whereas G_{rec} is reduced.

F. Carrier-to-Noise Ratio

Now suppose the broadband signal that is beamformed by the PAA receiver is a multi-carrier signal, with information channels with equivalent noise bandwidths B_{ch}. The CNR of one channel at the output of the two-port device then follows from Fig. 10 and the equations derived before as

$$
\mathrm{CNR} = \frac{G_{\mathrm{sys}}P_{\mathrm{in}}}{G_{\mathrm{rec}}k_{\mathrm{B}}T_{\mathrm{sys}}B_{\mathrm{ch}}} = \frac{G_{\mathrm{a}}}{T_{\mathrm{sys}}}\frac{P_{\mathrm{in}}}{k_{\mathrm{B}}B_{\mathrm{ch}}}
$$
$$
= \frac{P_{\mathrm{in}}G_{\mathrm{AE}}\eta_{\mathrm{t}}N}{k_{\mathrm{B}}(T_{\mathrm{a}} + T_{\mathrm{LNA}} + T_{\mathrm{OBF}}/(G_{\mathrm{LNA}}\Delta G))B_{\mathrm{ch}}}
$$
$$(36)$$

where T_{OBF} and ΔG are given by (30) and (35), respectively. We stress once more that this result only applies to systems where the AE signals have low CNRs, as explained in Section IV-E.

V. NUMERICAL EXAMPLE

As a numerical example, we consider a simplified version of the PAA receiver system that was designed in the SMART project, which was mentioned in the introduction. More specifically, consider the reception of television channels according to the Digital Video Broadcasting by Satellite (DVB-S) standard. In Europe, the power received per channel from for example the Astra satellite is known to be in the order of -150 dBW. Allowing a margin of 10 dB for fluctuating atmospheric conditions and changing location, we set the requirement for minimum detectable received power P_{in} to -160 dBW. The CNR at the input of a DVB-S receiver is required to be in the order of 8 dB. The brightness temperature of the sky around this satellite is in the order of 50 K, so we take $T_{\mathrm{a}} = 50$ K. A single AE will have a much wider antenna pattern than the complete PAA, and will therefore see radiating bodies as well. We assume that this results in AE temperatures $T_{\mathrm{AE}} = 150$ K. Suppose that commercial low-noise blocks (LNBs) are used to filter, amplify, and down-convert the AE signals prior to optical modulation, with gains $G_{\mathrm{LNA}} = 60$ dB, equivalent noise temperatures $T_{\mathrm{LNA}} = 50$ K, and equivalent noise bandwidths $B_{\mathrm{LNA}} = 1.2$ GHz. It then follows that the system noise temperature T_{sys} has a lower limit of $T_{\mathrm{a}} + T_{\mathrm{LNA}} = 100$ K. Assuming an equivalent noise bandwidth for the individual channels $B_{\mathrm{ch}} = 33$ MHz, we can derive from (36) that the minimum gain of the equivalent antenna G_{a} should be in the order of 34.6 dBi.

Suppose that we assume a planar array consisting of a rectangular grid of N equally weighted AEs (i.e., there is no amplitude tapering), with an inter-element spacing of half a wavelength. The latter is usually chosen in accordance with the *highest* frequency in the band of interest (12.75 GHz in our case), to avoid grating lobes at the lower frequencies. Therefore we assume an inter-element spacing of 1.18 cm. According to [54], the directivity of such an array is given by $G_{\mathrm{a}} = \pi N \cos(\theta)$, where θ is
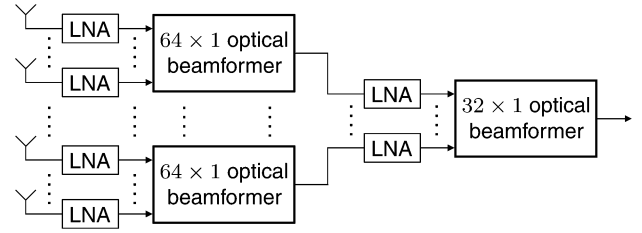

Fig. 11. Two-stage beamformer for a 2048-element antenna array, consisting of 32 parallel 64×1 beamformers in the first stage, whose output signals are combined by one 32×1 beamformer in the second stage.

the scan angle. (Strictly speaking this formula is only valid at 12.75 GHz, but, for simplicity, that is not considered in further detail here.) Considering a maximum scan angle of 60 degrees, it follows that the minimum number of AEs N should be in the order of 1830. Because of the structure of our beamformer, we round this to the next power of 2, so we take $N = 2048$, corresponding to a grid of 64×32 AEs. Note that this might not result in a satisfactory beam pattern (when it comes to beam width and sidelobe levels), but that is not considered in further detail here. In this paper the main focus is on analyzing the noise performance.

Now consider the beamformer. With our current technology [36], it is expected that one silicon wafer could accomodate an optical beamformer chip with at most 64 RF inputs. Therefore, we assume a two-level modular configuration as proposed in [14]. The total beamformer hence consists of 32 parallel 64×1 beamformers in the first stage, whose output signals are combined by one 32×1 beamformer in the second stage. Each beamformer in the first stage combines the signals of 64 AEs in one row of the PAA, whereas the beamformer in the second stage combines the combined signals from all rows. This is illustrated in Fig. 11.

The tuning ranges of the delays that are required in the beamformers follow from the geometry of the PAA. Since the AE spacing is 1.18 cm, the maximum delay between two neighbouring elements in one row of the PAA—incorporating a maximum scan angle of 60 degrees—is roughly 34 ps. Now suppose that each OBFN has a binary tree structure as depicted in Fig. 3. Then the first input port should have a fixed delay of 34 ps with respect to the second port (which could be implemented in the electrical domain, so that the lengths of the optical branches can be kept equal), and the second branch should have a delay element that can be tuned from 0 to 68 ps. This should be extended for the other ports, resulting in linearly increasing delay tuning ranges (up to $63 \cdot 68$ ps ≈ 4.3 ns for the 64th port). (Given the required optical bandwidth, this requires a certain number of rings, but that is not further considered here; see [36] for more details.) The 32×1 beamformer in the second stage is exactly the same, but requires fewer ports and hence a smaller maximum delay.

Apart from the chips, this requires $32 + 1 = 33$ lasers and balanced detectors, and the chips together contain $32 \cdot 64 + 32 = 2080$ modulators. Obviously, it is essential that components are chosen in the lower price range, in order to limit the total costs of the complete beamformer. Suppose lasers with an

output power of 10 dBm are used, so $P_o = 10$ mW. For simplicity, the power coupling coefficient κ of the coupler behind the laser is set to 1/2. Based on several recently reported results on high-speed compact MZMs, we assume here that, in the near future, it will be possible to integrate MZMs in our beamformers with a switching voltage V_π in the order of 1 V, and an optical excess loss L_m of roughly 2 dB. For the balanced detectors we assume photodiode responsivities R_{pd} of 0.8 A/W, and load impedances R_L of 50 Ω, which are at room temperature $T_0 = 290$ K. If we ignore the noise of any succeeding electronics, we find an RMS equivalent input noise current $I_{rms} = \sqrt{2kT_0/R_L} = 13$ pA/$\sqrt{\text{Hz}}$.

Further losses in the chip comprise the laser-chip and chip-detector losses, which we estimate to be in the order of 1 dB, so $L_{lc} = L_{cd} = 1.26$. The losses inside the chip, in the modulated path (L_{mp}) and unmodulated path (L_{up}), are dominated by the losses of the modulators (2 dB) and propagation losses in the waveguides. Although higher losses were measured in the chips that we present in [36], our partner, LioniX B.V., has already published optical chips with waveguide losses below 0.1 dB/cm [5]. Recently they have even measured losses in the order of 0.05 dB/cm, so we expect to realize beamformers with such loss characteristics in the very near future, and will therefore use that number in the calculation here. If we assume that the length of the unmodulated path is in the order of 5 cm, we find $L_{up} = 1.06$. The loss in the modulated path can be found from (16), with some additional assumptions. First, we assume that the splitters and combiners are lossless, so $\sum_n 1/L_{s,n} = \sum_n 1/L_{c,n} = 1$. Furthermore it is assumed that $L_{s,n} = L_{c,n}$, as this minimizes the loss. It is also assumed that the optical power is distributed over the branches in such a way that the differences in losses between the delay elements are compensated for, and uniform tapering is achieved. This can be done using (15). The losses in the ORR-based delays (in dBs) can be proven to be roughly equal to the effective optical path length times the loss coefficient [22], [25]. Hence, the worst case occurs when all the ORRs are tuned to their maximum delays. For example, the ORRs that are passed from the second input port of the 64×1 OBFNs introduce a maximum delay of 68 ps, which—assuming an effective group index of 1.55—corresponds to 1.3 cm, or 0.066 dB loss. This loss in dBs increases linearly for the other delay ports (resulting in 4.1 dB for the 64th port). Using (16) and the assumptions mentioned above, it can be proven that this gives a contribution of roughly 2.2 dB to the overall loss in the modulated path. For the 32×1 beamformer this becomes roughly 1.0 dB. If we use a filter structure as presented in [36], its size will be in the order of 5 cm, resulting in a passband loss of roughly 0.25 dB, so $L_f = 1.06$. When the fixed parts in the modulated paths (including the carrier re-insertion coupler) are also assumed to have a common length of roughly 5 cm, it follows that the total loss in the modulated path is roughly 4.7 dB ($L_{mp} = 3.0$) for the 64×1 beamformer and 3.5 dB ($L_{mp} = 2.2$) for the 32×1 beamformer.

Let us first consider the 64×1 beamfomers in the first stage. If we subsitute our parameters in (23), (24), (30), and (35), we find $G_{rec} = 200$ (23 dB), $T_{OBF} = 2.0 \cdot 10^7$ K, and $\Delta G = 0.9996$ (-0.002 dB). Apparently, the compression in the modulators is negligible, and the first beamformer stage gives a con-

tribution $T_{OBF}/G_{LNA} = 20$ K to the system noise temperature, which corresponds to an increase of 20%, or 0.8 dB reduction of the CNR. This could be improved by increasing the optical power (but this would require more expensive lasers), or by putting additional IF amplifiers behind the LNBs. The beamformer's contribution to the system noise temperature can be lowered to 1 K by inserting an IF gain of 13 dB. It can be verified that this still results in less than 0.1 dB of compression.

Now consider the 32×1 beamformer in the second stage. We can calculate that this beamformer has an effective input noise temperature of $7.5 \cdot 10^6$ K. First suppose that we would not put amplifiers between the first and second stage. Since the first stage has a total receiver gain of 36 dB (including the IF amplifier), it follows that this would give a contribution to the system noise temperature of $1.9 \cdot 10^3$ K. This can be decreased to 1 K by inserting IF amplifiers between the first and second stage with a gain of 33 dB (where the noise generated in these amplifiers is neglected). It can be verified that the compression is then still negligible.

Note that the assumption about the low optical losses is crucial here. Increasing them would decrease the intrinsic receiver gains G_{OBF} and hence increase the input noise temperatures T_{OBF} of the beamformers. This can be compensated for by increasing the amplification, but then the compression in the MZMs can become an issue.

VI. Conclusion

A novel beamformer concept has been introduced that enables squint-free, seamless steering of broadband receive PAAs, using integrated ORRs as broadband delay elements, filter-based optical SSB-SC modu中ltion for the E/O conversion, and balanced coherent optical detection for the O/E conversion.

The concept has potential for a very compact, low-weight implementation, by large-scale integration of the optical functionality (splitters, OBFN, OSBF, and carrier re-insertion), and hybrid integration with the laser, modulators, and the balanced detector. Hybrid integration of the modulators and the splitting and combining circuitry is essential in order to stabilize the phase relation between the optical signals that are combined in the OBFN.

Performance analysis has shown that the beamformer does not degrade the performance of the receiver system in which it is applied, provided that proper amplifiers are used, and that the optical losses are kept sufficiently low.

The feasibility of the system is also illustrated by experimental results on a (partly integrated) 8×1 optical beamformer setup in Part II of this paper [36].

References

[1] R. C. Hansen, *Phased Array Antennas*. New York: Wiley, 1998.

[2] R. A. Minasian, "Photonical signal processing of microwave signals," *IEEE Trans. Microwave Theory Tech.*, vol. 54, no. 2, pp. 832–846, Feb. 2006.

[3] A. J. Seeds and K. J. Williams, "Microwave photonics," *J. Lightwave Technol.*, vol. 24, no. 12, pp. 4628–4641, Dec. 2006.

[4] J. Capmany and D. Novak, "Microwave photonics combines two worlds," *Nature Photonics*, vol. 1, pp. 319–330, June 2007.

[5] F. Morichetti, A. Melloni, M. Martinelli, R. G. Heideman, A. Leinse, D. H. Geuzebroek, and A. Borreman, "Box-shaped dielectric waveguides: A new concept in integrated optics?," *J. Lightwave Technol.*, vol. 25, no. 9, pp. 2579–2589, Sept. 2007.

[6] N. A. Riza, *Selected Papers on Photonic Control Systems for Phased Array Antennas*, ser. SPIE Milestone. New York: SPIE, Jun. 1997, vol. MS 136.

[7] G. Grosskopf *et al.*, "Photonic 60-GHz maximum directivity beam former for smart antennas in mobile broad-band communications," *IEEE Photon. Technol. Lett.*, vol. 14, no. 8, pp. 1169–1171, Aug. 2002.

[8] A. P. Goutzoulis, D. K. Davies, and J. M. Zomp, "Hybrid electronic fiber optic wavelength-multiplexed system for true time-delay steering of phased array antennas," *Opt. Eng.*, vol. 31, no. 11, pp. 2312–2322, 1992.

[9] M. A. Piqueras *et al.*, "Optically beamformed beam-switched adaptive antennas for fixed and mobile broad-band wireless access networks," *IEEE Trans. Microwave Theory Tech.*, vol. 54, no. 2, pp. 887–899, Feb. 2006.

[10] D. Dolfi, P. Joffre, J. Antoine, J. P. Huignard, D. Philipper, and P. Granger, "Experimental demonstration of a phased-array antenna optically controlled with phase and time delays," *Appl. Opt*, vol. 35, no. 26, pp. 5293–5300, 1996.

[11] N. Madamopoulos and N. A. Riza, "Demonstration of an all-digital 7-bit 33-channel photonic delay line for phased-array radars," *Appl. Opt.*, vol. 39, no. 23, pp. 4168–4181, Aug. 2000.

[12] R. Soref, "Optical dispersion technique for time delay beam steering," *Appl. Opt.*, vol. 31, no. 35, pp. 7395–7397, Dec. 1992.

[13] R. D. Esman, M. Y. Frankel, J. L. Dexter, L. Goldberg, and M. G. Parent, "Fiber optic prism true time delay antenna feed," *IEEE Photon. Technol. Lett.*, vol. 5, no. 11, pp. 1347–1349, Nov. 1993.

[14] M. Y. Frankel, P. J. Matthews, and R. D. Esman, "Two-dimensional fiber-optic control of a true time-steered array transmitter," *IEEE Trans. Microw. Theory Tech.*, vol. 44, no. 12, pp. 2696–2702, Dec. 1996.

[15] R. A. Soref, "Fiber grating prism for true time delay beamsteering," *Fiber Integr. Opt.*, vol. 15, no. 4, pp. 325–333, Oct. 1996.

[16] H. Zmuda, R. A. Soref, P. Payson, S. Johns, and E. N. Toughlian, "Photonic beamformer for phased array antennas using a fiber grating prism," *IEEE Photon. Technol. Lett.*, vol. 9, no. 2, pp. 241–243, Feb. 1997.

[17] J. L. Corral, J. Marti, J. M. Fuster, and R. I. Laming, "Dispersion-induced bandwidth limitation of variable true time delay lines based on linearly chirped fibre gratings," *Electron. Lett.*, vol. 34, no. 2, pp. 209–211, Jan. 1998.

[18] B. Ortega, J. L. Cruz, J. Capmany, M. V. Andrés, and D. Pastor, "Variable delay line for phased-array antenna based on a chirped fiber grating," *IEEE Trans. Microwave Theory Tech.*, vol. 48, no. 8, pp. 1352–1360, Aug. 2000.

[19] D. B. Hunter, M. E. Parker, and J. L. Dexter, "Demonstration of a continuously variable true-time delay beamformer using a multichannel chirped fiber grating," *IEEE Trans. Microwave Theory Tech.*, vol. 54, no. 2, pp. 861–867, Feb. 2006.

[20] N. A. Riza, M. A. Arain, and S. A. Khan, "Hybrid analog-digital variable fiber-optic delay line," *J. Lighw. Technol*, vol. 22, no. 2, pp. 619–624, Feb. 2004.

[21] M. S. Rasras *et al.*, "Integrated resonance-enhanced variable optical delay lines," *IEEE Photon. Technol. Lett.*, vol. 17, no. 4, pp. 834–836, Apr. 2005.

[22] G. Lenz, B. J. Eggleton, C. K. Madsen, and R. E. Slusher, "Optical delay lines based on optical filters," *IEEE J. Quantum Electron.*, vol. 37, no. 4, pp. 525–532, Apr. 2001.

[23] J. E. Heebner, V. Wong, A. Schweinsberg, R. W. Boyd, and D. J. Jackson, "Optical transmission characteristics of fiber ring resonators," *IEEE J. Quantum Electron.*, vol. 40, no. 6, pp. 726–730, June 2004.

[24] L. Zhuang, C. G. H. Roeloffzen, and W. van Etten, "Continuously tunable optical delay line," in *Proc. 12th IEEE/CVT Symp. Benelux*, Enschede, The Netherlands, Nov. 3, 2005, paper P23.

[25] C. G. H. Roeloffzen, L. Zhuang, R. G. Heideman, A. Borreman, and W. van Etten, "Ring resonator-based tunable optical delay line in LPCVD waveguide technology," in *Proc. 10th IEEE/LEOS Symp. Benelux*, Mons, Belgium, Dec. 1–2, 2005, pp. 79–82.

[26] L. Zhuang, C. G. H. Roeloffzen, R. G. Heideman, A. Borreman, A. Meijerink, and W. van Etten, "Single-chip optical beam forming network in LPCVD waveguide technology based on optical ring resonators," in *Proc. Int. Topical Meeting on Microwave Photonics (MWP'2006)*, Grenoble, France, Oct. 3–6, 2006, paper F1.4.

[27] A. Meijerink, C. G. H. Roeloffzen, L. Zhuang, D. A. I. Marpaung, R. G. Heideman, A. Borreman, and W. van Etten, "Phased array antenna steering using a ring resonator-based optical beam forming network," in *Proc. 13th IEEE/CVT Symp. Benelux*, Liège, Belgium, Nov. 23, 2006, pp. 7–12.

[28] L. Zhuang, C. G. H. Roeloffzen, R. G. Heideman, A. Borreman, A. Meijerink, and W. van Etten, "Single-chip ring resonator-based 1 × 8 optical beam forming network in CMOS-compatible waveguide technology," *IEEE Photon. Technol. Lett.*, vol. 15, no. 15, pp. 1130–1132, Aug. 2007.

[29] L. Zhuang, A. Meijerink, C. G. H. Roeloffzen, D. A. I. Marpaung, J. Peña Hevilla, W. van Etten, R. G. Heideman, A. Leinse, and M. Hoekman, "Phased array receive antenna steering system using a ring resonator-based optical beam forming network and filter-based optical SSB-SC modulation," in *Proc. Int. Topical Meeting on Microwave Photonics (MWP'2007)*, Victoria, BC, Canada, Oct. 3–5, 2007, pp. 88–91.

[30] L. Zhuang, A. Meijerink, C. G. H. Roeloffzen, D. A. I. Marpaung, R. G. Heideman, M. Hoekman, A. Borreman, A. Leinse, and W. van Etten, "Novel ring resonator-based optical beamformer system and experimental results," in *Proc. 11th IEEE/LEOS Symp. Benelux*, Brussels, Belgium, Dec. 17–18, 2007, pp. 239–242.

[31] H. Schippers, J. Verpoorte, P. Jorna, A. Hulzinga, A. Meijerink, C. G. H. Roeloffzen, L. Zhuang, D. A. I. Marpaung, W. van Etten, R. G. Heideman, A. Leinse, M. Hoekman, and M. Wintels, "Broadband conformal phased array with optical beamforming for airborne satellite communication," in *Proc. IEEE Aerospace Conf. 2008*, Big Sky, MT, Mar. 1–8, 2008, paper 3.0102.

[32] H. Schippers, J. Verpoorte, P. Jorna, A. Hulzinga, L. Zhuang, A. Meijerink, C. G. H. Roeloffzen, D. A. I. Marpaung, W. van Etten, R. G. Heideman, A. Leinse, and M. Wintels, "Broadband optical beam forming for airborne phased array antenna," in *Proc. IEEE Aerospace Conf. 2009*, Big Sky, MT, Mar. 7–14, 2009, paper 3.0101.

[33] L. Zhuang, A. Meijerink, C. G. H. Roeloffzen, D. A. I. Marpaung, R. G. Heideman, M. Hoekman, A. Borreman, D. H. Geuzebroek, A. Leinse, and W. van Etten, "Experimental prototype of a novel ring resonator-based optical beamformer system," in *Proc. LEOS Ann. Mtg. 2007*, Lake Buena Vista, FL, Oct. 21–25, 2007, pp. 112–113, paper MM3.

[34] L. Zhuang, A. Meijerink, C. G. H. Roeloffzen, D. A. I. Marpaung, R. G. Heideman, M. Hoekman, A. Leinse, and W. van Etten, "Broadband phased array antenna steering by means of coherent signal combining in an integrated ring resonator-based optical beamformer," in *Proc. 13th IEEE/LEOS Symp. Benelux*, Enschede, The Netherlands, Nov. 27–28, 2008, pp. 71–74.

[35] L. Zhuang, A. Meijerink, C. G. H. Roeloffzen, D. A. I. Marpaung, R. G. Heideman, M. Hoekman, A. Leinse, and W. van Etten, "Novel ring resonator-based optical beamformer for broadband phased array receive antennas," in *Proc. LEOS Ann. Mtg. 2008*, Newport Beach, CA, Nov. 9–13, 2008, pp. 20–21, paper MB3.

[36] L. Zhuang, C. G. H. Roeloffzen, A. Meijerink, M. Burla, D. A. I. Marpaung, A. Leinse, M. Hoekman, R. G. Heideman, and W. van Etten, "Novel ring resonator-based integrated photonic beamformer for broadband phased array receive antennas—Part II: Experimental prototype," *J. Lightw. Technol.*, vol. 28, no. 1, pp. 19–31, Jan. 2010.

[37] G. P. Agrawal, *Fiber-Optic Communication Systems*. New York: Wiley, 1997.

[38] W. E. Stephens and T. R. Joseph, "System characteristics of direct modulated and externally modulated RF fiber-optic links," *J. Lightwave Technol.*, vol. 5, no. 3, pp. 380–387, Mar. 1997.

[39] C. H. Cox III, E. I. Ackerman, G. E. Betts, and J. L. Prince, "Limits on the performance of RF-over-fiber links and their impact on device design," *IEEE Trans. Microwave Theory Tech.*, vol. 54, no. 2, pp. 906–920, Feb. 2006.

[40] G. L. Abbas, V. W. S. Chan, and T. K. Yee, "A dual-detector optical heterodyne receiver for local oscillator noise suppression," *J. Lightwave Technol.*, vol. 3, no. 5, pp. 1110–1122, Oct. 1985.

[41] J. Park, W. V. Sorin, and K. Y. Lau, "Elimination of the fibre chromatic dispersion penalty on 1550 nm millimetre-wave optical transmission," *Electron. Lett.*, vol. 33, no. 6, pp. 512–513, Mar. 1997.

[42] G. H. Smith, D. Novak, and Z. Ahmed, "Technique for optical SSB generation to overcome dispersion penalties in fibre-radio systems," *Electron. Lett.*, vol. 33, no. 1, pp. 74–75, Jan. 1997.

[43] M. Sieben, J. Conradi, D. Dodds, B. Davies, and S. Walklin, "10 Gbit/s optical single sideband system," *Electron. Lett.*, vol. 33, no. 11, pp. 971–973, May 1997.

[44] S. Shimotsu, S. Oikawa, T. Saitou, N. Mitsugi, K. Kubodera, T. Kawanishi, and M. Izutsu, "Single side-band modulation performance of a LiNbO$_3$ integrated modulator consisting of four-phase modulator waveguides," *IEEE Photon. Technol. Lett.*, vol. 13, no. 4, pp. 364–366, Apr. 2001.

[45] M. Y. Frankel and R. D. Esman, "Optical single-sideband suppressed-carrier modulator for wide-band signal processing," *J. Lightwave Technol.*, vol. 16, no. 5, pp. 859–863, May 1998.

[46] A. Loayssa, C. Lim, A. Nirmalathas, and D. Benito, "Design and performance of the bidirectional optical single-sideband modulator," *J. Lightwave Technol.*, vol. 21, no. 4, pp. 1071–1082, Apr. 2003.

[47] R. Montgomery and R. DeSalvo, "A novel technique for double sideband suppressed carrier modulation of optical fields," *IEEE Photon. Technol. Lett.*, vol. 7, no. 4, pp. 434–436, Apr. 1995.

[48] K. Oda, N. Takato, H. Toba, and K. Nosu, "A wide-band guided-wave periodic multi/demultiplexer with ring resonator for optical FDM transmission systems," *J. Lightwave Technol.*, vol. 6, no. 6, pp. 1016–1023, June 1988.

[49] R. A. Griffin, D. D. Sampson, and D. A. Jackson, "Demonstration of data-transmission using coherent correlation to reconstruct a coded pulse sequence," *IEEE Photon. Technol. Lett.*, vol. 4, pp. 513–515, May 1992.

[50] N. M. Froberg, E. I. Ackerman, and C. H. Cox III, "Analysis of signal to noise ratio in photonic beamformers," in *Proc. IEEE Aerospace Conf. 2006*, Big Sky, MT, Mar. 4–11, 2006, paper 3.0604.

[51] A. Waldman and G. J. Wooley, "Noise temperature of a phased array receiver," *The Microwave Journal*, pp. 89–96, Sept. 1966.

[52] E. L. Holzman, "Intercept points of active phased array antenna," in *IEEE Microwave Theory Tech. Soc. Int. Microwave Symp.*, San Fransisco, CA, June 1996, pp. 999–1002.

[53] R. Meijerink, A. Meijerink, D. A. I. Marpaung, C. G. H. Roeloffzen, and W. van Etten, "Performance study of a ring resonator-based optical beam forming system for phased array receive antennas," in *Proc. 14th IEEE/CVT Symp. Benelux*, Delft, The Netherlands, Nov. 15, 2007, paper P16.

[54] B. J. Forman, "Directivity characteristics of scannable planar arrays," *IEEE Trans. Antennas Propagat.*, vol. 20, no. 3, pp. 245–252, May 1972.

Chris G. H. Roeloffzen (S'98-M'03) was born in Almelo, The Netherlands, in 1973. He received the M.Sc. degree in applied physics and Ph.D. degree in electrical engineering from the University of Twente, Enschede, The Netherlands, in 1998 and 2002, respectively.

From 1998 to 2002 he was engaged with research on integrated optical add-drop demultiplexers in silicon oxynitride waveguide technology, in the Integrated Optical MicroSystems Group at the University of Twente. In 2002 he became an Assistant Professor in the Telecommunication Engineering Group at the University of Twente. He is now involved with research and education on optical fiber communications systems. His current research interests include optical communications and RF photonic signal processing techniques.

Roland Meijerink (S'04) was born in Almelo, The Netherlands, in 1981. He received the M.Sc. degree in electrical engineering from the University of Twente, Enschede, The Netherlands, in December 2007. His master thesis was about the performance analysis of ring resonator-based optical beamformers. In February 2009 he received the M.Sc. degree in science education (cum laude), also from the University of Twente.

In 2001 he was a guest at Lucent Bell Labs Twente in Enschede, The Netherlands, working on QoS in rate-adaptive ADSL access networks, and in 2006 he was a guest at Ericsson Research in Research Triangle Park, NC, working on frequency domain adaptation in an OFDM system with channel feedback. In March 2009 he became a teacher in physics at the Herbert Vissers College in Nieuw-Vennep, The Netherlands.

Mr. Meijerink was a co-recipient of the 2000 Lucent Global Science Scholar award.
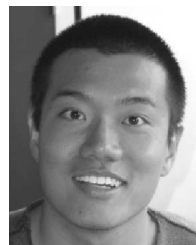
Leimeng Zhuang (S'05) was born in Beijing, China, in 1980. He received the B.Sc. degree in telecommunication engineering from the University of Electronic Science and Technology of China, Chengdu, China, in June 2003, and the M.Sc. degree in electrical engineering (with honours) from the University of Twente, Enschede, The Netherlands, in June 2005. His master thesis was about the time delay properties of optical ring resonators.

He is now working towards the Ph.D. degree in the Telecommunication Engineering Group at the University of Twente. His research is related to the development of ring resonator-based optical beam forming networks for phased array antenna systems.

Arjan Meijerink (S'00-M'06) was born in Almelo, The Netherlands, in 1976. He received the M.Sc. and Ph.D. degrees (both with honours) in electrical engineering from the University of Twente, Enschede, The Netherlands, in January 2001 and November 2005, respectively.

In 2000 he was a guest at Ericsson Business Mobile Networks in Enschede, developing error concealment techniques for Bluetooth voice links. From 2001 to 2005 he carried out his Ph.D. research on optical coherence multiplexing, in the Telecommunication Engineering Group at the University of Twente. He worked as a Postdoctoral Researcher in that same group from 2005 to 2007, carrying out research on RF photonic signal processing techniques, especially on the design and performance analysis of ring resonator-based optical beamformers. Since 2007 he has been an Assistant Professor in the Telecommunication Engineering Group, where he teaches an undergraduate course on random signals and noise, and is involved in research on new short-range radio transmission techniques for wireless adhoc networks. In 2009 he was a Visiting Lecturer in the Radio Communications Research Group at the Queen's University Belfast, Belfast, UK, working on the performance analysis of noise-based transmitted-reference systems in wideband fading channels.

Dr. Meijerink was a co-recipient of the Gauss Award for the best young researcher's presentation during the 22nd Symposium on Information and Communication Theory in the Benelux, in May 2001, and in July 2001, he was awarded the second prize in the IEEE Region 8 Student Paper Contest. He is a member of the Communication Society of the IEEE, and has acted as a reviewer for IEEE Photonics Technology Letters, and various conferences and symposia.

David A. I. Marpaung (S'05) was born in Balikpapan, Indonesia in 1979. He received the B.Sc. degree in physics (with honours) from Institut Teknologi Bandung, Indonesia, in 2002, and the M.Sc. degree in applied physics and the Ph.D. degree in electrical engineering, both from the University of Twente, Enschede, The Netherlands, in 2003 and 2009, respectively.

From 2005 to 2009 he was working on his Ph.D. research on performance enhancements of analog photonic links in the Telecommunication Engineering group, University of Twente. From July to October 2008 he was a guest researcher at the Netherlands Foundation for Research in Astronomy (ASTRON) working on gain enhancement and noise figure reduction of externally modulated analog photonic links, which will be used in a large-scale phased array antenna for radio astronomy purposes. He is now working as a postdoctoral researcher in the Telecommunication Engineering group, carrying out research on a large-scale photonic beamformer based on optical ring resonators.

Dr. Marpaung is a member of the Photonics Society of the IEEE, and has served as a reviewer for IEEE PHOTONICS TECHNOLOGY LETTERS.

Mark J. Bentum (S'92–M'95–SM'09) was born in Smilde, The Netherlands, in 1967. He received the M.Sc. degree in electrical engineering (with honours) from the University of Twente, Enschede, The Netherlands, in August 1991. In December 1995 he received the Ph.D. degree for his thesis "Interactive Visualization of Volume Data" also from the University of Twente.

From December 1995 to June 1996 he was a research assistant at the University of Twente in the field of signal processing for mobile telecommunications and medical data processing. In June 1996 he joined the Netherlands Foundation for Research in Astronomy (ASTRON). He was in various positions at ASTRON. In 2005 he was involved in the eSMA project in Hawaii to correlate the Dutch JCMT mm-telescope with the Submillimeter Array (SMA) of Harvard University. From 2005 to 2008 he was responsible for the construction of the first software radio telescope in the world, LOFAR (Low Frequency Array). In 2008 he became an Associate Professor in the Telecommunication Engineering Group at the University of Twente. He is now involved with research and education in mobile radio communications. His current research interests are short-range radio communications, novel receiver technologies (for instance in the field of radio astronomy), and sensor networks.

Dr. Bentum is a member of the Dutch Electronics and Radio Society NERG, the Dutch Royal Institute of Engineers KIVI NIRIA, and the Dutch Pattern Recognition Society. He has acted as a reviewer for various conferences and journals.

Maurizio Burla (S'08) was born in Orvieto, Italy, in 1982. He received his B.Sc. and M.Sc. degrees (both cum laude) from the University of Perugia, Italy, in 2005 and 2007, respectively. His M.Sc. thesis was on the design and realization of planar multiband antennas based on fractal architecture for Wireless-over-Fiber transceiver applications.

From December 2006 to April 2007 he was intern at Delta-Utec Space Research & Consultancy, Leiden, The Netherlands, among the YES2 (Young Engineers Satellite 2) project, in the RF subsystem integration and testing. In December 2007 he joined the System Engineering group at AleniaSIA S.p.A., Torino, Italy, working on the avionic system of Alenia C-27J Spartan aircraft. Since July 2008 he has worked at the Telecommunication Engineering Group of the University of Twente, Enschede, the Netherlands, as a Ph.D. student. His research focus is on advanced optical beamformers based on integrated optical ring resonators, and is part of the MEMPHIS project.

Mr. Burla was a co-recipient of the second Best Student Team Award at the International Astronautical Congress 2008, Glasgow, Scotland, for his work in the YES2 project.

Jaco Verpoorte was born in the Netherlands in 1966. He studied electrical engineering at the Eindhoven University of Technology, where he received the M.Sc. degree in 1991.

After his study he joined the National Aerospace Laboratory NLR in Marknesse, where he is still working as an R&D Manager in the field of electromagnetic technology. His current research activities include electromagnetic compatibility, antennas, and satellite navigation.

Pieter Jorna received the M.Sc. degree in applied mathematics from the University of Twente, Enschede, The Netherlands, in 1999, and the Ph.D. degree from Delft University of Technology, Delft, The Netherlands, in 2005.

From 1999 to 2005 he was with the Laboratory of Electromagnetic Research at Delft University of Technology, where he conducted research on the numerical computation of electromagnetic fields in strongly inhomogeneous media. Since 2005 he has been an R&D engineer with the National Aerospace Laboratory NLR in the Netherlands.

Adriaan Hulzinga was born in Wolvega, The Netherlands, in 1956. He received his B.Eng. degree in electronics from the Hogeschool Windesheim, Zwolle, The Netherlands.

Since 1996 he has been employed at the National Aerospace Laboratory NLR as a senior application engineer. He is involved in projects concerning antennas and electromagnetic compatibility.

Wim van Etten (M'80-SM'91) was born in Zevenbergen, The Netherlands, in 1942. He received the M.Sc. and Ph.D. degrees in electrical engineering from Eindhoven University of Technology, Eindhoven, The Netherlands, in 1969 and 1976, respectively.

From 1969 to 1970, he was with Philips Electronics, developing circuits for oscilloscopes. In 1970, he became an Assistant Professor at Eindhoven University of Technology, Faculty of Electrical Engineering. From 1970 to 1976, he was engaged in research on the transmission of digital signals via coaxial and multiwire cables. Since 1976, he has been involved with research and education on optical fiber communications. In 1985, he was appointed as an Associate Professor with Eindhoven University of Technology. In 1994, he became a Full Professor of telecommunications at the University of Twente, Enschede, The Netherlands, where he retired in 2007. His current interests include optical communications, mobile communications, detection, and simulation of communication systems. He is the author or coauthor of more than 140 papers in international journals, conferences, and symposia. He is the first author of *Fundamentals of Optical Fiber Communications* (Prentice Hall, 1991), and the author of *Introduction to Random Signals and Noise* (Wiley, 2005). Two of his papers were selected for a collection of 57 key papers on communications that appeared in the last 50 years in IEEE ComSoc publications (*The Best of the Best: Fifty Years of Communications and Networking Research*, Wiley, 2007).

Prof. Van Etten is a member of the Dutch Institute of Electronic and Radio Engineers (NERG). He is a member of the executive committee of the IEEE Benelux joint Chapter on Communications and Vehicular Technology, and vice-chairman of the executive committee of the IEEE Benelux Section. He has been a member of organizing committees and program committees of various conferences and symposia.